TAMPEREEN TEKNILLINEN YLIOPISTO
TAMPERE UNIVERSITY OF TECHNOLOGY

HAMASA FAQHIRI

CHITOSAN AND SILICA BIOACTIVE GLASS 3D POROUS COMPOSITE FOR TISSUE ENGINEERING

Master of Science Thesis

Examiners: Professor Minna Kellomäki, Dr. Jonathan Massera (Docent, Assistant professor, Academy Research Fellow) and Dr.Teresa Rebelo Calejo.
Thesis was approved by the academic Board at 8 of June 2016

ABSTRACT

Hamasa Faqhiri: Chitosan and Silica Bioactive Glass 3D Porous Composite for Tissue Engineering

Tampere University of Technology
Master of Science Thesis, 44 pages
December 2016
Master's Degree Programme in Material Engineering
Major: Biomaterials
Examiners: Professor Minna Kellomäki, Dr. Teresa Rebelo Calejo, Jonathan Massera (Docent, Assistant professor, Academy Research Fellow)

Keywords: chitosan, bioactive glass, composite scaffold, tissue engineering, bone regeneration, silica glass, S53P4

The aim of the study was to fabricate and characterize three-dimensional (3D) chitosan and bioactive glass composite scaffolds. Chitosan, as a natural polymer has suitable properties for tissue engineering applications, and combining it with bioactive glass, known to promote bone regeneration, evoked promising results.

Chitosan-Bioactive glass composites were made by dissolving chitosan in acetic acid, and adding the bioactive glass to the solution until reaching uniform content. Three glass contents were tested in this project. The porous 3D composite scaffolds were made using freeze drying method. Sodium hydroxide (NaOH) was used as neutralizing agent to remove the acidity from the scaffold. The actual glass content, within the scaffolds, was evaluated by thermogravimetry analysis, and change in the sample porosity and mechanical properties evaluated as a function of glass content. Scaffolds were immersed in TRIS buffer solution for ten different time points (from 6 hours to 5 weeks). After immersion, the sample mass loss and water uptake was quantified. The solution was analysed based on changes in pH and Ca^{2+} concentration. The mechanical properties of the wet samples were tested to mimic more accurately the *in-vivo* conditions.

Chitosan has a spongy structure with cylindrical pores. The porosity was found to decrease with increasing the glass content. Compressive strength was measured at 50% strain and was found to increase with the glass content. However, both the compressive strength and the elastic modulus showed a maximum at 29 wt% of glass introduced in the chitosan matrix. Immersion in TRIS buffer solution clearly led to degradation of the composite. With adding the glass particles, a rise in pH was noticed, attributed to the leaching of ions from the glass to the surrounding. This was further confirmed with the increasing calcium concentration within the immersion medium. For prolonged immersion time infrared spectroscopy seemed to indicate precipitation of a hydroxyapatite layer, which was not evenly distributed at the surface of the composites. Wet mechanical testing was found to lead to lower elastic modulus and compressive strength than when tested dry. However, the heavy swelling of the samples was also found to lead to high inaccuracy in the measurements.

TIIVISTELMÄ

Hamasa Faqhiri: Kudosteknologinen kitosaanin ja bioaktiivisen lasin huokoinen 3D-komposiitti
Tampereen Teknillinen Yliopisto
Diplomityö, 44 sivua
Joulukuu 2016
Materiaalitekniikan diplomi-insinööri tutkinto-ohjelma
Pääaine: Biomateriaalit
Tarkastaja: Professori Minna Kellomäki, PhD Teresa Rebelo Calejo, Akatemiatutkija, dosentti Jonathan Massera

Avainsanat: kitosaani, bioaktiivinen lasi, komposiitti, kudosteknologia, luonnonpolymeeri

Tutkimuksen tavoitteena oli valmistaa ja karakterisoida huokoisia ja kolmiulotteisia kitosaanin ja bioaktiivisen lasin komposiitteja. Luonnon polymeerina kitosaanilla on lupaavia ominaisuuksia kudosteknologiaan. Kirjallisuudesta tiedetään,että bioaktiivisen lasin lisääminen polymeeriin yleensä lisää luun regeneroitumista. Kudosteknologisissa implanteissa huokoisiin tukirakenteisiin (skaffoldeihin) yleensä yhdistetään soluja, jotta voidaan ylläpitää tai palauttaa vammautuneen kudoksen tai elimen toiminta.

Tässä työssä kitosaanin ja bioaktiivisen lasin (S53P4) komposiitti saatiin valmistettua liuottamalla kitosaania etikkahapossa ja lisäämällä bioaktiivista lasia liuokseen, kunnes saavutettiin homogeeninen koostumus. Huokoiset 3D-komposiittirakenteet saatiin valmistettua liuoksesta pakastekuivauksella. Natriumhydroksidia (NaOH) käytettiin neutraloivana aineena poistamaan happamuutta skaffoldeista. Tutkin työssäni kolmea eri painoprosenttia bioaktiivisen lasin pitoisuutta. Lopullinen lasipitoisuus skaffoldeissa arvioitiin termogravimetrianalyysin (TGA) avulla, ja muutokset näytteen huokoisuudessa ja mekaanisessa lujuudessa arvioitiin lasimäärän funktiona. Skaffoldeja hydrolysoitiin TRIS-puskuriliuoksessa ja näytteitä tarkasteltiin kymmenessä eri ajankohdassa kuudesta tunnista viiteen viikkoon. Hydrolyysin jälkeen näytteen massahäviö ja veden absorptio määritettiin. Liuoksesta analysoitiin pH:n ja Ca^{2+}-konsentraation muutoksia. Mekaaniset lujuusominaisuudet näytteistä tutkittiin märkänä, jolloin matkittiin mahdollisimman todenmukaisesti *in vitro* -olosuhteita. Hydroksiapatiitin muodostumista skaffoldien pinnalla tutkittiin FTIR-menetelmällä.

Kylmäkuivauksella kitosaaniin muodostui sienimäinen rakenne, missä huokoset olivat lieriömäisiä. Huomattiin, että huokoisuus väheni suhteessa ja verrannollisesti lasipitoisuuden kasvaessa. Kompressiovoima mitattiin 50% rasituksessa ja tarvittava voima kasvoi lasipitoisuuden kasvaessa kuitenkin siten, että elastinen modulus oli suurimmillaan näytteessä, missä oli 29 painoprosenttia bioaktiivista lasia. FTIR-tutkimuksessa huomattiin hydroksiapatiittiin viittaavia kemiallisia sidoksia, jotka osoittavat tutkitulla kitosaanin ja bioaktiivisen lasin komposiitilla olevan potentiaalia luun kudosteknologiaan.

PREFACE

This Master of Science thesis was performed in the Biomaterials and Tissue Engineering group in the Department of Electronics and Communication Engineering at Tampere University of Technology.

First of all, I would like to address my appreciation and gratitude to professor Jari Viik for introducing me to Dr. Jonathan Massera. I express my endless gratitude to Dr. Jonathan Massera for offering me the opportunity to do my master thesis under his supervision. I am very honoured and grateful to be supervised by him, without his guiding, support and teaching this project would have not been possible. I thank from my heart Dr. Teresa Rebelo Calejo for her supervision and being in contact with me, even, when she was in her maternity leave. I thank professor Minna Kellomäki and all the Biomaterials and Tissue Engineering group for their kindness and support throughout the thesis process. Special thank goes to Sanna Karjalainen for her co-operation on mechanical testings and being a supportive friend during this journey.

I want to thank my parents Saleha and Hashem Faqhiri and my loved brother Abdullah Roman Faqhiri for their unconditional love, support and patience throughout my studies. Last but not least, I would like to thank all my family and friends and all the master students spending the year 2016 with me in the laboratory and TUT MSc office.

Tampere, 14.12.2016

Hamasa Faqhiri

CONTENTS

LIST OF FIGURES

LIST OF SYMBOLS AND ABBREVIATIONS

3D	Three-dimensional
AAS	Atomic absorption spectroscopy
ATR	Attenuated total reflectance
BAG	Bioactive glass
$CaCl_2$	Calcium chloride
CaO	Calcium oxide
CO_3^{2-}	Carbonate
CT	Computed tomography
DI	Deionized
DTA	Differential thermal analyzer
FDA	Food and Drug Administration
FTIR	Fourier transform infrared spectroscopy
HCl	Hydrochloride, hydrochloric acid
IR	Infrared
mol%	Mole percent
P_2O_5	Phophorous pentoxide
PCL	Polycaprolactone
SD	Standard deviation
SEM	Scanning electron microscope
SiOH	Silanol
SiO_2	Silicondioxide
SBF	Simulated body fluid
NaOH	Sodium hydroxide
Na_2O	Sodium oxide
t	Thickness
TGA	Thermogravimetry analysis
TRIS	Tris(hydroxymethyl)aminomethane
wt%	Weight percent

1. INTRODUCTION

The role of tissue engineering is getting more important, to treat people through regeneration of damaged tissue. In tissue engineering, scaffolds are usually fabricated and combined with cells in order to be used to maintain or restore the function of a diseased part of the body. Bioactive glass and its polymers composites play an important role in the field of bone tissue engineering. Numerous researches have been made to design and fabricate safe and suitable substitutes for bone tissue (Soumen 2012; Escobar-Sierra et al. 2015).

Scaffolds with the needed shape, size, porosity and functionality are vital to allow the cells to grow into specific tissues. Scaffold microstructure should mimic the structure of the native tissue with suitable pore size allowing transport of nutrients and waste products. The mechanical properties of the scaffold should also be similar to the native tissue. Taking into account the challenge in obtaining scaffolds with adequate microstructure, developing new suitable biomaterials is of the upmost importance. (Rahaman et al. 2011).

The aim of this research project was to produce and characterize 3D composite scaffolds based on a natural polymer and silicate bioactive glass. Chitosan was selected as the natural polymer and S53P4 as the bioactive glass. Chitosan is non-toxic, biocompatible, biodegradable and bioadhesive (Jayakumar et al. 2010). Chitosan is easy to fabricate into gels, membranes, nanofibers, beads, micro- and nanoparticles, scaffolds and sponges. Its properties allow applications in tissue engineering such as wound healing and drug and/or gene delivery (Jayakumar et al. 2010). However, chitosan is known to have weak mechanical properties, which minimizes its use in applications requiring higher load. Bioactive glass, can, on the other hand, improve the mechanical strength of chitosan (Caridade et al. 2013) and its bioactivity allows formation of chemical bonds with bone and soft tissue (Peter et al. 2010; Caridade et al. 2013). Silicate bioactive glass, S53P4 is Food and Drug Administration (FDA) approved, (Massera et al. 2012), allowing safe application in biological systems. As a result of its osteostimulative properties, bioactive glass is used as bone regenerative material. When introduced in physiological fluid, glass particles degrade leading to the formation of a silica layer and release of alkali and alkaline earth ions within the surrounding medium. The release of Ca^{2+} ions leads to a supersaturation and physiological medium instability at the vicinity of the glass. This instability, in turns, leads to the precipitation of a calcium-phosphate layer, in the form of amorphous hydroxyapatite, at the glass surface. Precipitates of calcium-phosphate crystallize as hydroxyapatite over time, which is important for bone regeneration (Cerruti et al. 2005a; Peter et al. 2010). Combination of both materials properties, trough processing of a composite materials, may allow the design of improved scaffolds for tissue engineering applications.

The purpose of the study was to develop a porous composite scaffold with a chitosan matrix and S53P4 bioactive glass as filler. The amount of filler was varied and impact of glass filling content on the main properties of the composites were investigated. *In-vitro* dissolution test in TRIS buffer solution was carried out, for immersion times up to 840 hours (5 weeks). The physical, structural and mechanical properties of the composites were discussed as a function of immersion time and correlated to the chitosan and bioactive glass dissolution.

In this thesis, the state of the art is presented. This section includes basics on glass and chitosan dissolution and medical applications, as well as, general properties of both materials when use separately. Previous work on chitosan/bioactive glass composited and the main results obtained will be discussed. In the following section, materials and detailed methods used for this study are presented. The results obtained are discussed in light of the requirement for a 3D scaffolds. The pore size, mechanical properties and dissolution behavior is discussed based on the glass content in the composites. The glass content was estimated by thermogravimetric analysis. During dissolution change in the immersion solution pH was recorded and correlated to ions from the glass leaching out. Degradation of the composites was assessed via Fourier transform infrared spectroscopy (FTIR) and the samples mechanical properties were estimated in compression using a Instron mechanical tester. The conclusion of this project will highlight the strength and weaknesses of the composites developed, based on the requirements for an optimum scaffold.

2. THEORETICAL BACKGROUND

Natural polymers are formed in nature during natural growth cycles. Polysaccharides, i.e. starch and cellulose, and proteins are examples of natural polymers (Vroman & Taghzert 2009). Biopolymers are referred to the natural biodegradable polymers. Natural polymers often have similarities to extracellular matrix providing good biological performance as well as controlled degradation. Polysaccharides possess hemocompatibility while having lower cost than the other natural polymers making them attractive materials for tissue engineering purposes. (Pishbin et al. 2011).

Bioactive glasses (BAG) are bioactive surface reactive ceramic biomaterials, mainly consisting of silicon dioxide (SiO_2), sodium oxide (Na_2O), calcium oxide(CaO) and phosphorus pentoxide (P_2O_5) (Hench 1991). Bioactive glasses require SiO_2 composition lower than 60% to become bioactive. In addition, bioactive glasses must contain high sodium oxide (Na_2O) and calcium oxide(CaO) as well as high CaO/P_2O_5 ratio (Massera 2015). Bioactive glasses were first developed by Hench, and the most studied one is Bioglass®, which is used in clinical treatment. (Boccaccini et al. 2010; Rahaman et al. 2011). In this study silicate bioactive glass S53P4 was combined with a natural polymer, chitosan, to produce porous composites.

2.1 Chitosan

Chitosan is natural polysaccharide, obtained by deacetylation of chitin. Chitin is the supporting material of crustaceans and insects consisting of 2-acetamido-2-deoxy-β-D-glucose units linked through β-(1→4) linkages (Ravi Kumar 2000). Chitosan, on the other hand, is linear cationic polysaccharide consisting of β-(1→4)-linked glucosamine and N-acetyl-D-glucosamine (Pishbin et al. 2011). The structure of the chitin and chitosan is shown in Figure 2.1 (Ravi Kumar 2000).

Formation of chitosan from chitin is presented schematically in Figure 2.1 (Ravi Kumar 2000). Chitosan is made by deacetylation of chitin, which is obtained from shells of crustaceans such as carbs. Usually shells are crushed into powders and treated with sodium hydroxide (NaOH). Obtained powder is neutralized and demineralized with HCl. Further powders are deacetylated with NaOH and dried to obtain chitosan. (Escobar-Sierra et al. 2015; Ravi Kumar 2000).

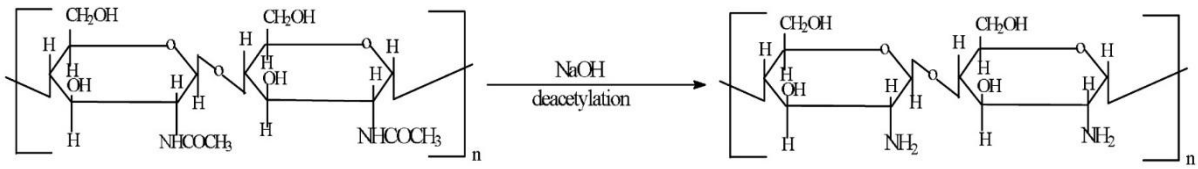

Figure 2.1 *Formation of chitosan from chitin (Ravi Kumar 2000)*

Chitosan degrades with lysozymes or chitosanase (Vroman & Tighzhert 2009). Degradation of the chitosan starts with the rapid weight loss and water adsorption. Amorphous region of the chitosan is more accessible for the lysozyme and water permeates into the crystalline zone. The crystalline zone degrades by lysozyme. (Jayakumar et al. 2010). Degradation rate depend on degree of deacetylation and molecular weight (Ren et al. 2005a; Soumen 2012). Ren et al. reports that with ~80% degree of acetylation, *in vivo* degradation rate of chitosan is ~5% / week (Ren et al. 2005a).

Properties:

Chitosan is soluble in dilute acid such as acetic acid and formic acid (Ravi Kumar 2000). It has low cost and is available in large scale (Jin et al. 2008). Chitosan has been reported to have good biocompatibility, biodegradability, non-antigenicity, anti-tumour activity, anti-inflammatory effect, antimicrobial activity, protein adsorption properties and ability to accelerate wound healing (Bui et al. 2011). Chitosan has rigid and compact crystalline structure making it insoluble in water and alkaline solutions (Vroman & Tighzhert 2009). Chitosan has similar structure to glycosaminoglycans, which are the major component of bone and cartilage. Therefore, it favours cell adhesion allowing attachment, differentiation and morphogenesis of osteoblasts (Peter et al. 2010; Bui et al. 2011). However, since it is mechanically weak and unstable as well as showing heavy swelling upon immersion, chitosan is not able to maintain its predefined shape for transplantation (Jin et al. 2008).

To improve chitosan mechanical properties, composites of chitosan with hydroxyapatite, β-tricalciumphosphate, and montmorillonite can be prepared (Peter et al. 2010). Another method to improve unstable and weak mechanical properties of chitosan is by cross-linking with other polymer (Jin et al. 2008). Chitosan can be cross-linked with or combined with other polymers such as gelatin, alginate, poly(lactic acid), collagen, as well as with hyaluronic acid, peptides and hydroxyapatite. Scaffolds have been prepared to treat tissues such as cartilage, bone, skin and disks. (Namatsku et al 2006).

Chitosan is easy to fabricate into gels, membranes, nanofibers, beads, micro- and nanoparticles, scaffolds and sponges (Jayakumar et al. 2010). The versatile properties of chitosan allow multiple applications in biotechnology, tissue engineering and other applications. However, only applications and fabrication methods used for bio- and tissue

engineering will be presented in this chapter, with emphasis being given to chitosan composites and scaffolds for bone tissue regeneration.

2.2 Bioactive glass

Silica bioactive glasses was developed by L.L. Hench (Hench 1991). This type of glass is surface reactive and is bioactive, i.e. it has the ability to form bonds with bone tissue in physiological environment. The classic bioactive glass 45S5 is known as Bioglass®, which has a composition (in wt. %) of 45% SiO_2, 24.5% Na_2O, 24.5% CaO, and 6% P_2O_5. Bioactive glasses can have a large variety of composition. They may contain additional ions with specific therapeutical abilities such as fluorine (F), magnesium (Mg), strontium (Sr), iron (Fe), silver (Ag), boron (B), potassium(K) or zinc (Zn). Bioactive glasses can be produced by traditional melting and quenching process or using the sol-gel approach. (Boccaccini et al. 2010; Rahaman et al. 2011).

The S53P4 bioactive glass (BonAlive Biomaterials Ltd., Turku, Finland) has a composition (in wt. %) of 53% SiO_2, 4% P_2O_5, 23% Na_2O, and 20% CaO. S53P4 glass is Food and Drug Administration (FDA) approved (Boccaccini et al. 2010; Massera et al. 2012; Rahaman et al. 2011). As van Gestel at al reports the use of S53P4 is increasing in bone graft applications. S53P4 bioactive glass is shown to facilitate and stimulate bone formation and bone defect healing. (van Gestel et al. 2015). The S53P4 has shown antibacterial effect on several different bacterial strain without the need of special antibacterial ions. The antimicrobial properties were attributed to the rise in pH observed upon bioactive silicate glass composition. (Zhang et al. 2010; van Gestel et al. 2015). Antibacterial effects of glass are dependent on the dissolution mechanism of BAG and amount of the alkali released. This is more prominently seen in nanometric glass particles, as they release higher amount of alkaline species displaying stronger antimicrobial effect. (Zhang et al. 2010).

BAG has ability to bind to both soft and hard connective tissues (Rahaman et al. 2011). It is osteoconductive, osteostimulative, having the ability to promote cell adhesion and proliferation (Peter et al. 2010; van Gestel et al. 2015). Surface reactive properties of BAG ensure deposition of calcium phosphate layer when immersed in physiological medium (van Gestel et al. 2015). The structure of BAG can be changed to target specific functions by changing its composition, such as slower *in vitro* dissolution rate. Slower degradation rate might be beneficial for healing larger bone defects. (Massera *et al.* 2012). Degradation and surface reaction of BAG is shown in Figure 2.2.

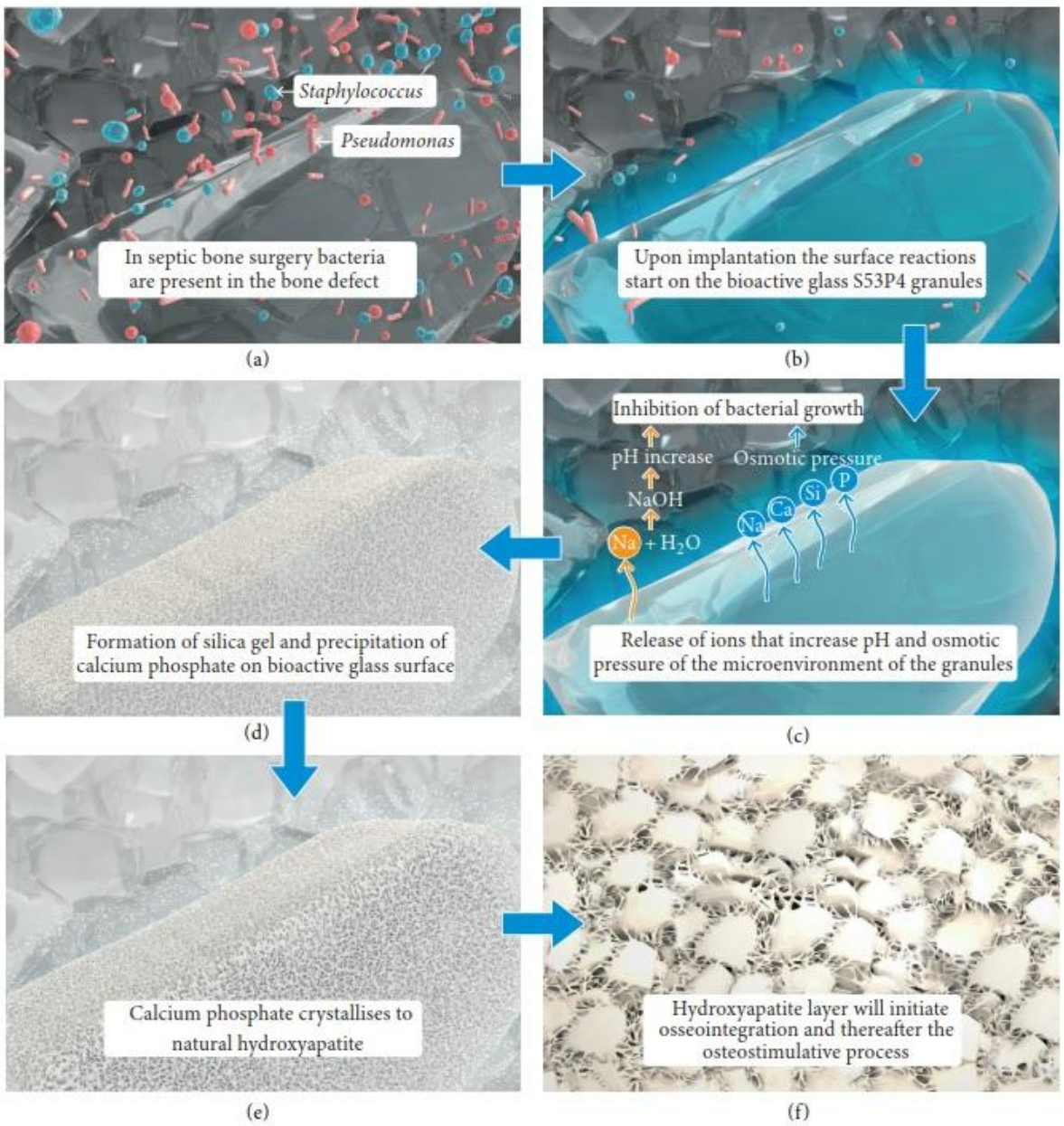

Figure 2.2 *Surface reactions of bioactive glass. (van Gestel et al. 2015)*

As soon as BAG is immersed in the physiological solution, the dissolution of ions and soluble species such as Na^+ and Ca^{2+} ions start taking place. Rapid ion exchange rises the pH of the solution, and Si-OH groups forms at the material's surface. Degradation is followed by loss of the soluble silica as $Si(OH)_4$ by breakage of the Si-O-Si bridging links. Surface silanol groups tend to form a SiO_2-rich layer and migration of Ca^{2+} and PO_4^{3-} causes formation of a calcium-phosphate rich layer at the surface of BAG. Ca-P layer further crystalizes with carbonate groups to form hydroxyapatite on the surface of the glass and/or scaffold. (Rahaman et al. 2011; Bui et al. 2011).

2.3 Composites of chitosan and bioactive glass

Caridade et al. compares micro- and nano-sized bioactive glass particles with chitosan in terms of bioactivity, mechanical and structural properties. For their study 5µm and 30-50nm particle sizes were used. Composite membranes were prepared by solvent casting and were thereafter immersed in stimulated body fluid (SBF). The size of the inclusions affects the mechanical properties of the material, as it influences interactions between polymer and filler particles. (Caridade et al. 2013)

Bui and co-workers report that chitosan-bioactive glass composite can be promising materials for bone tissue engineering. Composites of chitosan and 46S6 bioactive glass was prepared by freeze-drying. The paper reports the crystallization of apatite layer on the surface of the chitosan-BAG composite. Porous structure and high surface area to volume of the composite provides ion transport from physiological fluid, forming a dense apatite layer. Calcium and phosphorus concentration, within the medium, shows rapid increase in the beginning of the immersion period and then decrease gradually with time due to the Ca-P layer formation. At the end of the immersion period (30 days) the phosphorus concentration was zero, as all the phosphorus was consumed to form hydroxyapatite. Calcium ion release was higher in the BAG and lower in the chitosan-BAG composite. (Bui et al. 2011).

Peter et al fabricated chitosan-BAG scaffolds by cross-linking it with glutaraldehyde. Ultrasonication was applied to the solution in order to reduce particle size. Once again nanosized particles were used in this study. Nanocomposites of BAG and chitosan were prepared by lyophilisation. Scaffolds showed adequate porosity for cell attachment and spreading. Addition of the bioactive glass allowed controlled swelling and degradation. (Peter et al. 2010).

Maji et al prepared chitosan-gelatin-bioglass 3D porous scaffolds by freeze-drying. In their study, 20-30 nm glass particles were used, and scaffolds with various glass compositions were immersed in phosphate buffer solution to study materials' bioactivity and biodegradability. Scaffold reported to be highly porous and having excellent biodegradability. Mechanical properties were examined by compression strength and scaffolds with 30 weight percent showed maximum of compressive strength at 2.2 MPa. Addition of BAG improves compressive strength of the material. Cell studies showed cell growth within 14 days, providing promising results for bone grafts. (Maji et al. 2016).

In another study, Bioglass® 45S5 was fabricated by foam replication and coated with chitosan and polycaprolactone (PCL). Coating of the scaffolds was obtained by freeze-drying method. It is reported that addition of the Bioglass® improves mechanical strength of the scaffolds. (Yao et al. 2014).

3. MATERIALS AND METHODS

Chitosan and bioactive glass S53P4 composites were prepared by freeze-drying to obtain 3D porous scaffolds. Properties of the scaffolds were studied as such and after *in vitro* dissolution test. Surface porosity was investigated by optical microscopy and structural analysis was done by Fourier transform infrared spectroscopy (FTIR). *In vitro* dissolution test was performed in TRIS buffer solution to study degradation and bioactivity of the produced scaffolds. To detect formation of hydroxyapatite or apatite layer formation on the scaffolds, FTIR and ion release test were carried out. Mechanical properties of the chitosan and chitosan-bioactive glass composites were compared, before and after *in vitro* test. Detailed methodology used is described in this chapter.

3.1 Sample preparation

Scaffold were prepared in four stages: preparation of bioactive glass, preparation of chitosan solution, addition of BAG powder into the chitosan solution and freeze drying to produce composites with porous structures.

3.1.1 Glass preparation

Silica bioactive glass, S53P4, was melted from batches containing mixtures of sand (99.4 % pure SiO_2), and analytical grades of Na_2CO_3, $CaCO_3$, and $CaHPO_4.2H_2O$. The used glass composition in mol% is presented in table 1.

Table 3.1 *S53P4 glass composition*

Glass composition	**SiO_2**	**Na_2O**	**CaO**	**P_2O_5**
mol%	53.86	22.66	21.77	1.72

The glass was melted in air, in a platinum crucible at 1400°C for 3 hours. The glasses were then casted into a graphite mold. Successively the ingots were annealed and then crushed into powders with <50 µm and 125-250 µm sizes.

3.1.2 Chitosan/ glass composite preparation

Chitosan solution was made using chitosan powder supplied by Acros Organics with molecular weight: 100 000 – 300 000 g/mol. For this work, 2 weight percent (wt-%) chitosan

was dissolved in 1% acetic acid (Peter et al. 2010). Solutions were stirred using a magnetic stirrer (RO5, IKA® -Werke GmbH &Co. KG, Germany) until complete dissolution of the chitosan. The viscous solutions were left to stir slowly (30 rpm) overnight to set and prevent bubble formation.

Composite scaffolds containing 25wt-%, 50wt-% and 75wt-% BAG composite were prepared as follow. BAG S53P4 (< 50 µm) was slowly added to the chitosan solution while stirring. The glass was added slowly to prevent aggregate formation. The pure chitosan solution (with no glass particles) was labelled as 0wt-% and was used as the control in this study. All the prepared solutions were poured onto 30 ml, 107×25mm Sarstedt plastic test tubes. Each test tube contained 25 ml of the solution for consistency. Samples were frozen overnight and freeze-dried at -100 – -110 °C for 48 hours, using a freeze-dryer (CT/DW 110, Heto Drywinner, Jouan Nordic, Denamrk).

As chitosan is dissolved in acetic acid, the scaffold was assumed to be slightly acidic. After being freeze-dried, samples were neutralized using 0.2 M sodium hydroxide (NaOH). Test tubes with samples were filled with 0.2 M NaOH and left at room temperature for 30 minutes. The sodium hydroxide solution was poured away and samples were washed using distilled water until reaching neutral pH. The pH was checked with pH test strips. Samples were frozen overnight and freeze-dried again for 24 hours. (Peter et al. 2010)

The obtained 3D scaffolds were cut into discs (thickness t = 5 mm) using clean shaving blades. The shaving blades was found to be the best available cutting tools compared to scalpel blades to produce slices without modifying the pore structure. As the glass and the chitosan are known to be reactive to moisture, all the samples were maintained in a dry desiccator before further analysis.

3.2 Characterization of composites

3.2.1 Porosity

Optical microscopy was used to qualitatively study the microstructure and morphology of the as produced composites. An optical microscope (Zeiss SV8, Carl Zeiss, Germany) was used with 0.8 × objective. As the surface of the sample was thick, and light did not pass through it, an additional lamp (KL1500, Schott, Germany) was used to illuminate the samples from the top rather than from the bottom. Pictures were taken using a microscope camera (BUC2-500C, BestScope, China) and saved for later analysis.

3.2.2 Thermal properties

Thermal analysis was done using a thermal analyzer (STA 449 F1 Jupiter, Netzsch, Germany). Using the combined thermogravimetric (TGA) and differential thermal analyzer (DTA) one can simultaneously record the change in mass and in enthalpy occurring as the

temperature increases. Three parallel samples from edge and three from center were studied for each batch of composite prepared. Figure 3.1 shows a photograph of the scaffolds, illustrating where the center and edge of the sample are located.

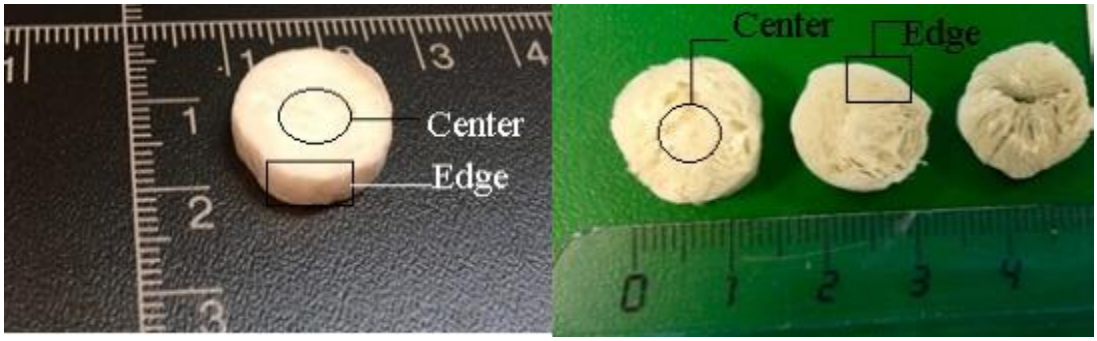

Figure 3.1 *Location of center and edge of the samples*

All tests were performed in alumina (Al_2O_3) crucible under nitrogen (N_2) atmosphere. The N_2 flow was set to 20 mL/min for the purge and 50 mL/min for the protective atmosphere. Samples were heated from 20 to 1200 °C, at rate of 10 °C/min. The obtained data were analyzed using Proteus Analysis and Origin 8 software. A typical TGA graph defining the residual mass of the samples, as referred to glass content, is presented in Figure 3.2.

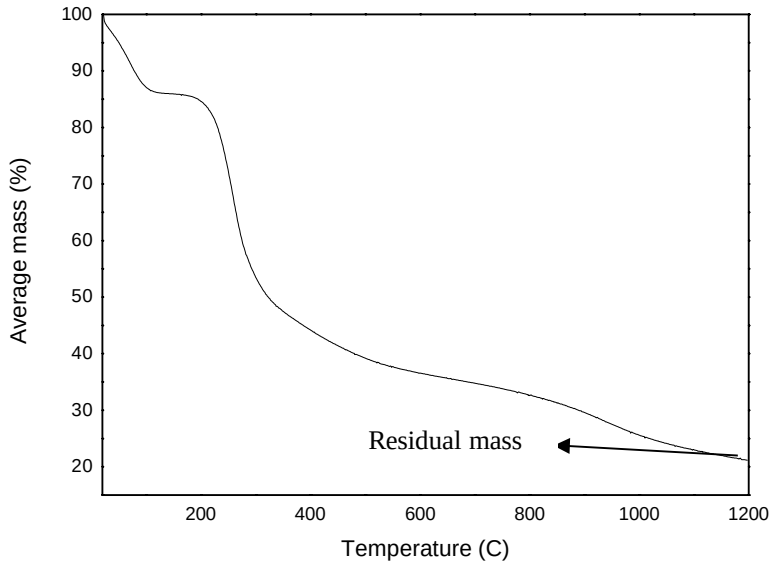

Figure 3.2 *Typical TGA graph showing the residual mass of the sample*

3.2.3 Mechanical properties

The impact of glass content on the mechanical properties of the composites was studied in compression using an Instron ElectroPluse E1000, High Wycombe, UK. Height and area of the samples were measured with a digital calliper (Absolute Digimatic calliper series 500,

Mitutoyo, USA) and the data entered into the Instron software. Four parallel samples were studied in compression test. To correct for the uneven surface, samples were initially compressed until a smooth surface was reached, in order to provide maximum contact between instrument compression plates and samples. Samples were compressed to 50% of their height at 1 mm/min rate. Load string stiffness was applied by the instrument itself, and specific value, for each sample separately, was given by the Instron software. The data was collected and analysed later on Microsoft Office Excel and Origin8 software. Samples were studied as dry and wet, respectively. To study wet compression strength of the samples, two parallel samples were immersed in TRIS buffer solution for 5 minutes and compressed as previously described. When possible, the compression strength at fracture or the load at 50% deformation were quantified.

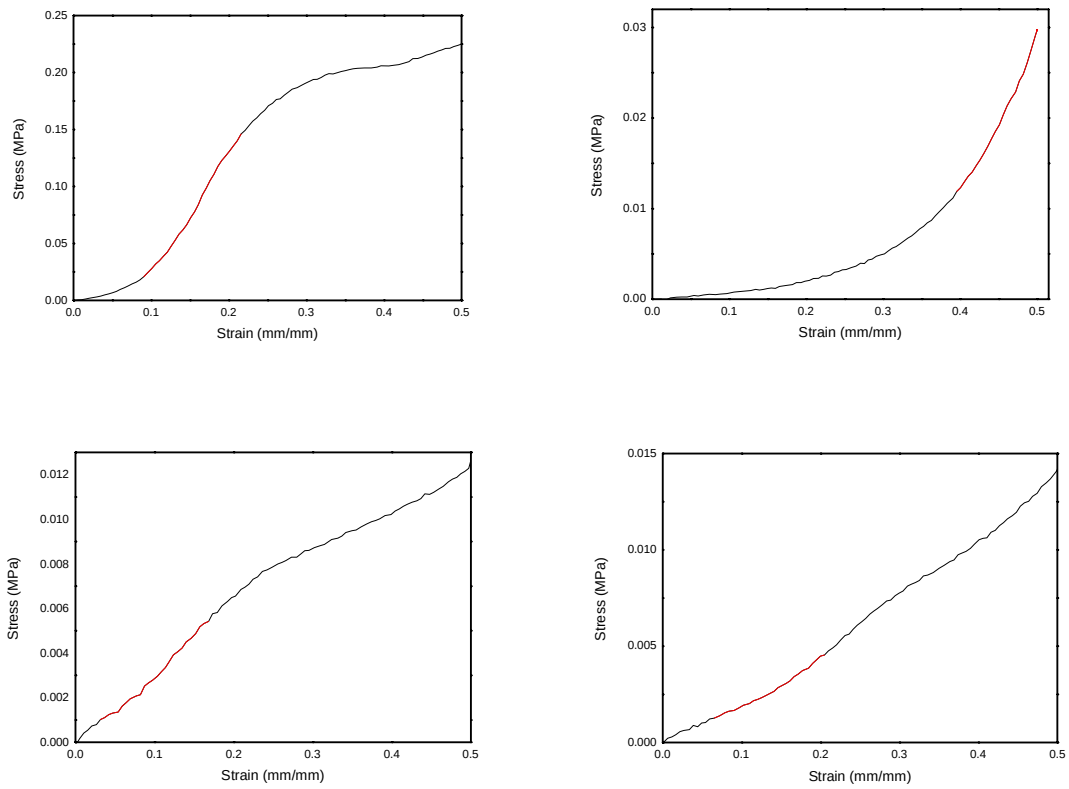

Figure 3.3 *Elastic region on the stress-strain curve depending on the curve shape*

Young's modulus was calculated form the slope/elastic part of the stress -strain curve, shown in the Figure 3.3. In the graphs red line shows the elastic region, which varies depending on the shape of the obtained curves. In this study, parallel samples were analysed and the average was calculated. The standard deviation corresponds to the min and max of the obtained value.

3.2.4 Structural properties

Fourier transform infrared spectroscopy (FTIR) was used to study sample structure. An FTIR (Spectrum One FT-IR Spectrometer, Perkin Elmer, Perkin Elmer instruments, USA) was

used in attenuated total reflectance mode (ATR). The crystal used was a diamond. The resolution used was 4 cm^{-1}, number of accumulated scans was 8, and studied range was 650 – 4000 cm^{-1}. The data were collected and analysed using Origin8 software. All spectra were baseline corrected and normalised to the band with maximum intensity.

Two parallel samples were used from edge and two from center (Figure 3.1) of the same sample, leading to four samples analyzed for each type of composite. If the sample had bubbles as a result of swelling, the bubbles were also studied.

3.3 *In-vitro* dissolution test

In vitro immersion test was done for all three composites sample and the chitosan control. Time points were selected as: 0, 6h, 24h, 48h, 72h, 1 week, 2 weeks, 3 weeks, 4 weeks and 5 weeks. Triplicates of each sample were analyzed for each time point. In this study, Tris(hydroxymethyl)aminomethane (TRIS) by Trizma® was used as a buffer solution. Procedure described by Sigma Aldrich was followed to obtain 1 liter of 0.05M TRIS buffer solution, pH 7.40. Temperature was kept at 37°C. The solution was then poured into a graduated flask, and deionized (DI) water was added to reach 1liter mark. The solution was stored in the fridge until next day and its pH was checked again. The accepted pH change for TRIS solution left in the fridge is ± 0.02.

Samples were placed on individually labelled test tubes, and their initial weight was measured using an analytical scale (Mettler Toledo AG 245, Mettler Toledo, Switzerland). TRIS buffer solution was added to the samples. The volume of TRIS solution was calculated based on the individual dry mass of the specimen in order to maintain a constant surface area to volume of TRIS ratio (SA/V), as proposed in (Orava et al., 2007). One blank sample (containing only TRIS) was also prepared as control for each time point to ensure that any variation in pH was due to the composite degradation rather than change in the TRIS solution with time. Samples were placed in the shaking incubator (Multitron AJ 118g, Infors, Bottmingen, Switzerland) at 100 rpm, 37°C. At each time point, samples were taken out of the incubator, immediately placed in a warm water bath (TW80, Julabo, Germany) set at 37°C and their pH measured with an accuracy of ± 0.02. The pH change was compared with the reference TRIS solution.

5 ml was taken from the buffer solution and was diluted to 50 ml. These diluted solutions were stored in the fridge for calcium release studies. The immersed composites were taken out of the buffer solution, rinsed with distilled water, and their wet masses measured. Immediately after weighting, samples were prepared for mechanical test, after which they were frozen in the freezer at temperature -100 – -110ºC.

3.3.1 Mass loss and water uptake

Immediately after the composite samples were removed from the immersing solution, they were gently placed on dry tissue to remove the excess TRIS solution, rinsed with DI water and then weighted. The water uptake or water absorption can be calculated using the following equation (1) (Orava et al. 2007):

$$\text{Water absorption } (\%) = 100 \times (m_1 - m_2)/m_2 \quad (1)$$

Where m_1 is the wet weight measured after the immersion period, and m_2 is the dry mass of samples.

Samples were then frozen and dried at -100 – -110°C using the freeze-dryer for 24 hours. After that, samples were placed in the vacuum chamber (WTB Binder 78532, Tuttlingen, Germany) for another 24 hours. Dry masses of samples were measured and their mass loss was calculated using equation (2) (Orava et al. 2007; Peter et al. 2010).

$$\text{Mass loss } (\%) = 100 \times (m_0 - m_2)/m_0 \quad (2)$$

Where, m_0 is the initial weight of the samples before immersion; and m_2 is the dry mass of samples.

3.3.2 Calcium release

Calcium release was investigated using atomic absorption spectroscopy (AAnalyst 300 Atomic Absorption Spectrometer, Perkin Elmer instruments, USA). The used wavelength was 422.7 and slit was 0.70 mm. This system uses an oxy-acetylene flame. Standard solutions with known calcium (Ca^{2+}) content (1mg/l, 2mg/l, 5mg/l and 7.5 mg/l) were prepared and measured to obtained a master calibration curve. AAwinlab software was used to produce the calibration curve. The calibration curve was used to calculate the calcium content (mg/ml) of the immersion solutions from the corresponding absorbance data. The immersing solution stored were then analysed and the absorbance obtained compared to the master curve. It is well known that an oxyacetylene flame does not dissociate efficiently all the compound being release by the bioactive glass and thus a 10% error was expected.

3.3.3 Structural properties

FTIR was used to study samples' structural properties. After the *in vitro* dissolution test, samples' structure was examined to see how the dissolution affected the structure of the scaffolds. Similar procedure than the one described in chapter 3.2.4, was used.

3.3.4 Mechanical properties

The impact of the immersion on the mechanical properties of the scaffolds was analysed for both wet and dry samples, essentially as described in section 3.2.3. After *in vitro* dissolution testing, samples were gently rinsed with DI water, weighted and their area and height was measured. Wet samples were placed in the compression device, shown in Figure 3.4, left. Samples were frozen and freeze-dried as described in 3.1.2 Freeze-dried samples were similarly analysed (right of the Figure 3.4).

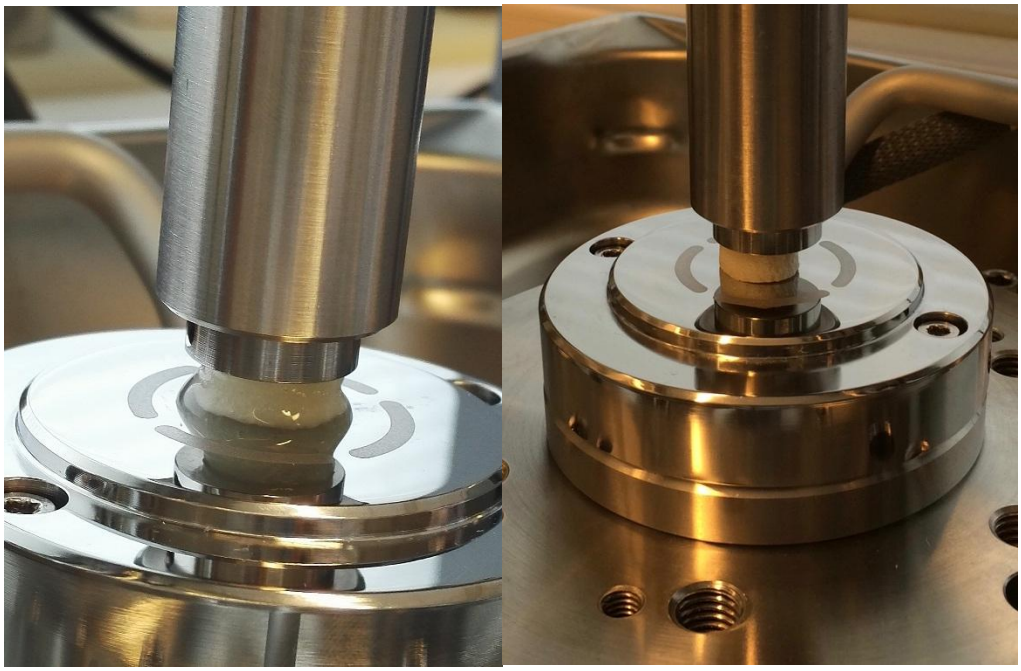

Figure 3.4. *Compression test of the wet (left) and dried (right) composite samples.*

3.4 Statistical analysis

All the results were obtained from triplicate or duplicate samples depending on the experiment performed. Data are expressed either as mean ± standard deviation (SD) or mean ± min/max values, respectively.

4. RESULTS AND DISCUSSIONS

Freeze-drying of chitosan control and chitosan/bioactive glass, containing various amount of glass, was conducted to obtained composite scaffolds. The physical, mechanical, morphological and microstructural properties of the samples were studied and results are reported in this section. The final glass content, in weight %, in the composites was assessed using thermogravimetric analysis. The samples microstructure (porosity) was studied using optical microscopy. Change in the strain/stress curve obtained in compression will be discussed as a function of glass content, as well as the change in the samples elasticity as a reflected by the Young's modulus. Finally, the structural properties of the composites were examined with FTIR and compared to a chitosan control.

The bioactivity of the material, *in vitro,* was carried out in TRIS buffer solutions. The dissolution / degradation of the samples is discussed based on i) pH change, ii) mass loss, iii) water uptake and iv) Ca^{2+} release. Change in the samples structures was recorded as a function of immersion time using FTIR.

4.1 Chitosan/glass composites

Chitosan solution (2% concentration) had a clear yellow colour, which became turbid after the addition of glass (Figure 4.1). In the first experiments, BAG with particle size 120 - 150mm was used. However, due to the high density of the glass (2.60 g/cm^3), the large size of the particles led to particles sinking at the bottom of the test tube. As such, < 50 mm BAG particles were subsequently used in the fabrication of the scaffolds. Even then, glass particles in suspension (as shown in Figure 4.1) were observed to sink to the bottom of the test tubes, when let to set for some minutes. Therefore, after complete dispersion of BAG while slowly stirring, all solutions were immediately placed in the freezer at –20ºC to prevent sinking of the bioactive glass particles. Sample size was found to decrease after freeze-drying to almost half of their height and to diameter of Ø=10mm. In addition, after freeze-drying, colour difference between chitosan and chitosan-BAG composites was still visible by eye. After neutralizing and freeze-drying, sample size changes from 10mm to 6.50-7.50mm in diameter and from 250 mm to 100-150 mm in height. Samples were cut into discs (t = 5 mm, Ø = 6.50 – 10 mm) as shown in Figure 4.2. The scaffolds have a spongy texture, and returned to their shape when pressed lightly. This was more noticeable while cutting the chitosan samples. Scaffolds containing BAG were hard but brittle compared to chitosan scaffolds. Chitosan contains layered structure with cylindrical pores, when observed with naked eye.

Figure 4.1 *Pure chitosan and chitosan-BAG composites solutions*

Controlling the pore size of the samples was found difficult. The presence of small bubbles will lead to undesired large pores in the structure. In addition to chitosan, chitosan-BAG with the lowest content of glass also had larger pores at the bottom of the sample batch, possibly due to the presence of air bubbles in the chitosan solution and possible over pressure during freeze-drying. Nonetheless, such samples were removed from the test series, whereas samples without large pores were cut and stored in the dry desiccator for further characterization. Samples containing increasing amount of glass particles were found to be harder and easier to handle.

Figure 4.2 *Porous scaffolds of chitosan-BAG 75wt% composite samples.*

4.2 Composites characterization

Studying composite properties and comparing them to the chitosan control allows us to observe the effect of BAG on the properties of the scaffolds. Samples are characterized in term of thermal, topographic, and mechanical properties as well as structural properties.

4.2.1 Thermal properties

Glass content of the composites and thermal degradation of all scaffolds were studied by thermogravimetry and differential thermal analysis (TGA/DTA). From the parallel repeats

of each composite type, one average graph was plotted in Origin8. Figure 4.3 shows the thermogravimetric curve for chitosan control and chitosan-BAG composites, corresponding to the change in mass as a function of temperature.

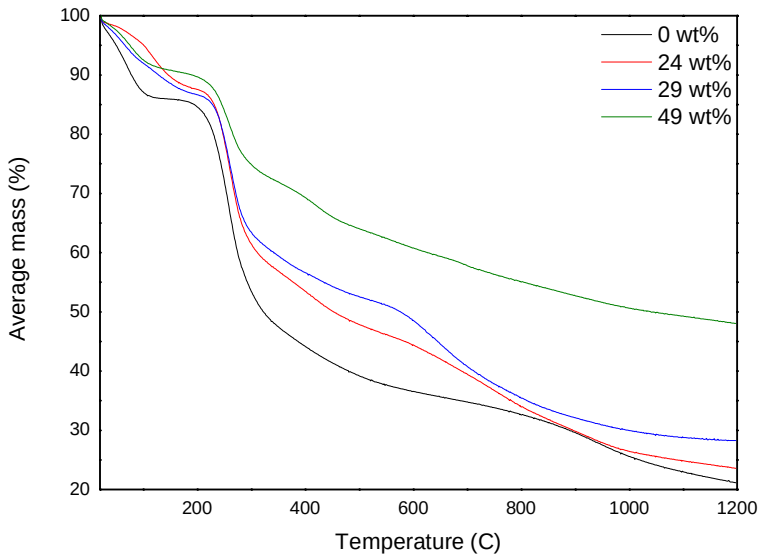

Figure 4.3 *Thermogravimetric analysis of chitosan and chitosan-BAG composites*

Degradation stages can be observed in the TGA-curve of the 2wt% chitosan control labelled as 0wt%. Under nitrogen atmosphere, 15% mass loss happens at 100 ºC. This first stage corresponds to the evaporation of water bonded to the polymer, which means that water is physically absorbed and/or weakly bounded to chitosan molecules via hydrogen bonds (de Britto & Campana-Filho 2007; Zawadzki & Kaczmarek 2010; Georgieva et al. 2012). The second stage starts at about 200ºC and extend within the 200 ºC – 400 ºC temperature range, where dehydration, deacetylation and depolymerization of the chitosan chains takes place. The third stage occurs at temperatures higher than 400 ºC and refers to the decomposition of pyranose rings trough dehydration and deamination and finally ring opening (Zawadzki & Kaczmarek 2010). The rest of the thermal degradation associates to residual decomposition reactions and burning of the volatile compounds (de Britto & Campana-Filho 2007; Georgieva et al. 2012). Residual mass in the chitosan control (0wt%) is ~20% of the original mass. In the case of composite samples, residual mass is expected to correspond to the glass particles present in the samples. The theoretical glass content in the composites was 25wt-%, 50wt-% and 75wt-%. Estimated/ “actual” glass content of chitosan-BAG 25wt-%, chitosan-BAG 50wt-% and chitosan-BAG 75wt-% were measured to be 24wt-%, 29wt-% for and 49wt-%, respectively The measured glass content is used in the label of the various composites and is reported in Table 4.1. The table summarizes the difference between the estimated and the expected glass content with accuracy of the measurement corresponding to the standard deviation of the parallel repeats. However, one should keep in mind that the residual mass in the measured using TGA, for the composites, do not correspond only to the

glass content but to the glass content and residue of chitosan. This suggests that the actual glass content in the composites are lower than measured.

Table 4.1 *Expected versus estimated glass content in composites*

Expected glass content	**Obtained glass content**	**Sample label**
25 wt-%	24 wt-% ± 5	chitosan-BAG 24wt-%
50 wt-%	29 wt-% ± 5	chitosan-BAG 29wt-%
75 wt-%	49 wt-% ± 15	chitosan-BAG 49wt-%

The **Error! Reference source not found.**, also, show that the degradation mechanism of chitosan changes in the presence of glass. Table 4.2 present the mass change and temperature domain for each degradation stage.

Table 4.2 *Degradation stages of the chitosan control and chitosan-BAG composites*

Degradation	**Changes**	**0wt-%**	**24wt%**	**29wt%**	**49wt-%**
1st stage	Mass loss	15%	10%	15%	<10%
	Temperature (ºC)	100	150	200	100
2nd stage	Mass loss	~40-45%	~40%	~35%	~25%
	Temperature (ºC)	200-300	200 – 300	200 - 400	200 –250
3rd stage	Mass loss	~70%	>50%	~50%	~35%
	Temperature (ºC)	400-800	300-600	400-600	450

With increasing the glass content one can see that the first stage of degradation, related to removal of absorbed water remain fairly constant. However, the second stage of chitosan degradation, while occurring at similar temperature range, showed lower mass loss for increasing glass content. This is only attributable to the lower content of chitosan in the composite compared to the chitosan control samples. Lastly, the third stage not only presented lower mass loss with increasing glass content but also a degradation shifted to lower temperature, indicating that the presence of glass and lower content of chitosan favour the thermal degradation of chitosan.

Despite using the small size (<50 µm) significant sinking of the particles was noticed. These was further evident with increasing the BAG particles content as particles will tend to agglomerate and formed larger mass sinking at a faster rate. Such behavior leads to large glass particle content distribution along the length of the prepared rose. This was particularly evident for chitosan-BAG 49wt-% scaffolds, it was visually observable that glass particles sank significantly to the bottom of test tube. The heterogeneity of the glass particles' distribution drastically increased for the larger BAG content as can be seen from the error of the measurement and most likely due to particles agglomeration.

4.2.2 Porosity

Chitosan control showed spongier structure compared to the chitosan-BAG composites. Freeze-dried chitosan contains layered structure. Cutting the scaffolds into thin discs, allows us to see the spongy but feathery structure of the scaffold. The surface structure of the samples, with long and cylindrical pores, is represented in the optical microscopy images, Figure 4.4. Pore shape was not even and differed within the same sample type: some were deep and long, whereas others were long but not deep.

Glass particles appear as bright spots in the optical microscopy images. Therefore, in Figure 4.4 (a), there are no bright spots, as chitosan control (0wt-%) does not contain any glass particles. However, in the Figure 4.4 (b), (c) and (d) bright spots are visible, proving presence of the glass particles. Porosity in the chitosan samples was difficult to control, and after freeze-drying and neutralizing, the pores inside the sample could be even up to 500µm. Adding bioactive glasses to the chitosan was found to lead to smaller pores and lower overall porosity. Both chitosan-BG 24wt-% and 29wt% has at least a couple of large pores of 400-500µm, where chitosan-BAG 49wt% did not contain any large pores.

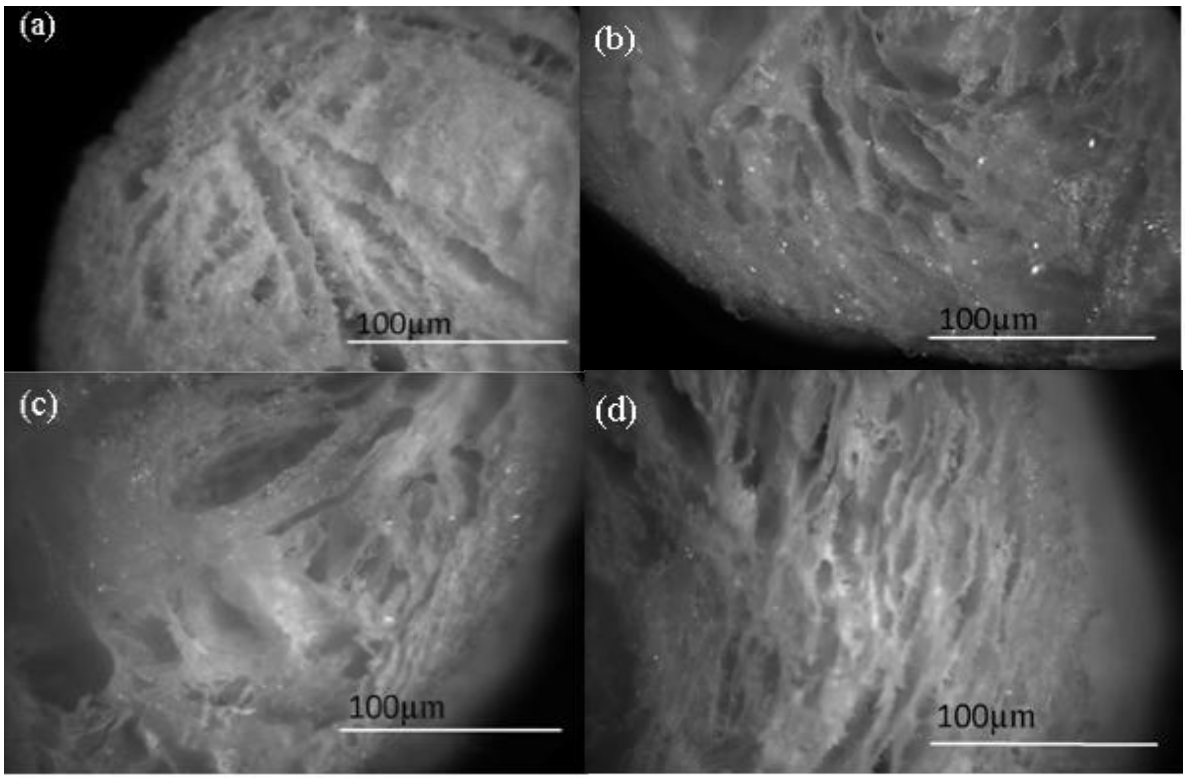

Figure 4.4 *Optical microscopy image of (a) chitosan control, (b) chitosan-BAG 24wt-%, (c) chitosan-BAG 29wt-%, (d) chitosan-BAG 49wt-%.*

Using only optical microscopy sample with 24 and 29 wt-% of BAG seem to have similar pore size and pore size distribution. Conversely, scaffolds containing 49wt-% has smaller pore size, which is visible in the optical microscopy, Figure 4.4 (d). Pore sizes of the samples have an important effect on the characteristics of the scaffolds, as they influence the flow speed of substances through the scaffold. Nevertheless, it is difficult to completely characterize the porosity of the sample, based simply on its surface structure and surface porosity. In future work, additional experiments should thus be carried out such as scanning electron microscope (SEM) and/or computed tomography (CT) in order to optimally characterize the samples and predict substance flow.

4.2.3 Mechanical properties

The stress-strain curve (Figure 4.5) was plotted as an average curve from the obtained data, and the mechanical properties of the chitosan control were compared to the composite scaffolds when compressed to 50% of their original height.

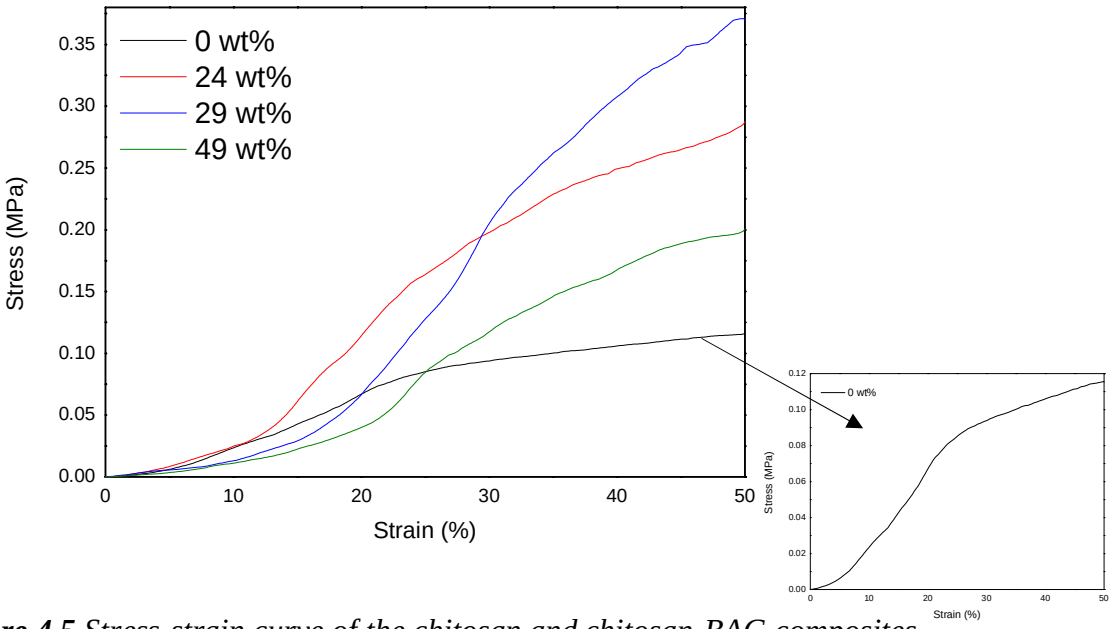

Figure 4.5 *Stress-strain curve of the chitosan and chitosan-BAG composites*

The stress-strain curve shows that addition of the bioactive glass increases the compressive strength. As expected, chitosan-BAG composite 24wt-% demonstrated higher compressive strength compared to chitosan control, but lower compressive strength compared to chitosan-BAG 29wt-%. The difference between chitosan-BAG 24wt-% and 29wt-% is hence a result of the higher glass content. In a similar fashion, the composite with higher glass content (49wt-%) was expected to show higher compressive strength than the scaffolds with lower BAG content. However, Figure 4.5 shows the opposite i.e. that the scaffold demonstrated lower compressive strength compared to other composites.

The stress-strain curve of the chitosan scaffold is similar to the one reported by Madihally & Matthhew (Madihally & Matthew 1999) for similar chitosan. When adding glass, the stress-strain relation changes. However, not all the obtained stress-strain curves followed one trend (Figure 3.3). The location of the elastic region differed even within the same parallel samples. Some results showed elastic and plastic deformation of the sample. First, scaffolds have setting region, then the elastic region, from which the Young's modulus is calculated, and the plastic region. Similar mechanical response of chitosan has been reported earlier by (Soumen 2012). Similarly, no fracture point was detected. Compressing scaffolds to 50% of their height did not show fracture point, thus compressing the samples to higher strength would allow to investigate when material breaks. Average value and standard deviation for the Young's modulus and for the compressive strength at 50% deformation were calculated and are summarized in Table 4.3

Table 4.3 *Tensile strength and Modulus of chitosan and chitosan-BAG composites*

Sample label	Tensile Strength (MPa)	Young's Modulus (MPa)
chitosan 0wt-%	0.12 ± 0.06	0.23 ± 0.05
chitosan-BAG 24wt-%	0.29 ± 0.05	0.44 ± 0.09
chitosan-BAG 29wt-%	0.4 ± 0.2	0.782 ± 0.007
chitosan-BAG 49wt-%	0.2 ± 0.3	0.25 ± 0.16

There is an increase in compressive strength and Young's modulus, when introducing bioactive glass into the chitosan scaffolds. Both parameters increase, when glass content increases. Chitosan-BAG 49wt-% was found to have lower tensile strength and Young's modulus compared to the two other composite types. As explained previously, this is due to an uneven distribution of glass particles, which effects on the stiffness of the material. Also it is possible that the first increase in stress, up to 20% compression, in the composite containing the highest amount of BAG is an artefact from a hard, uneven surface.

4.2.4 Structural properties

Structural properties of the samples were analyzed using FTIR. Figure 4.6 shows infrared (IR) spectra of chitosan control and chitosan-BAG composites. Typical absorption band position correlated to the chitosan and bioactive glass structure are summarized in the Table 4.4and Table 4.5.

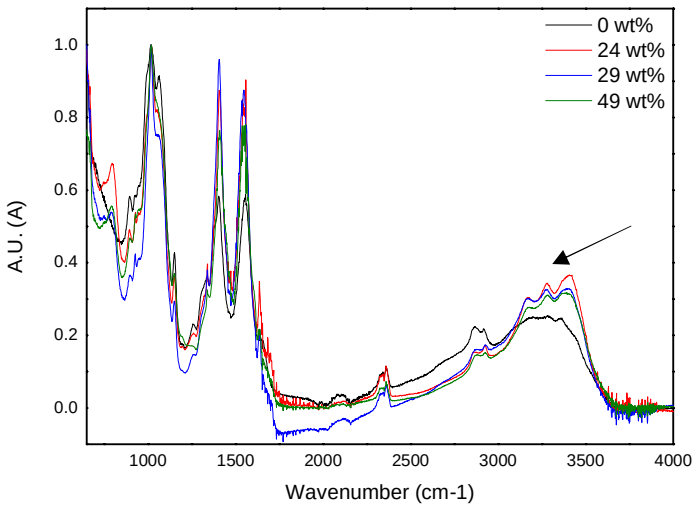

Figure 4.6 *Structural properties of the chitosan and chitosan-BAG composite scaffolds*

Table 4.4 *Assignation of FTIR absorption bands of bioactive glass**

Wavenumber (cm^{-1})	**Identification of absorption bond**
3670, 3672, 4500	Hydroxyl band
3425 -5400, 1611	Water absorption in silica glass
2800	Water-enriched glass
1876, 1431, 1638	Absorbed water molecules in the pores
1076, 800-809	Si–O–Si stretching, Si–O– stretching vibration group
540, 758, 745, 932, 1036	Si–O–Si bending, Si-O bind in every SiO_4
503	Si-O-Si deformation
1092, 836	SiO_2 asymmetric vibration, SiO_2 symmetric vibration
1020	Si-O-Si and P=O
653, (1022), 660, 462	PO_4 (presence of v_4 PO_4), PO_4
602, 962	P-O stretching, P-O symmetric stretching
564	P-P ending vibration
590	O-P-O bending vibration
900-1200	Presence of SiO and PO
828, 878, 1409, 1638	Carbonate (CO_3^{2-})
1460, 875	C-O stretching, vibration of carbonated hydroxyapatite

* (Cerruti et al. 2005b; de Britto & Campana-Filho 2007; Zawadzki & Kaczmarek 2010; Bui et al. 2011; Caridade et al. 2013; Yao et al. 2014; Maji et al. 2016)

Table 4.5 *Assignation of FTIR absorption bands of chitosan**

Wavenumber (cm^{-1})	**Identification of absorption bond**
3496 – 3440, 3345, 3370	OH and -NH_2 groups, O–H band overlaps N–H band
1377	O-H and N-H axial stretching, NH-stretching vibration
2910, 2913, 2859	C-H stretching
1300, 2926, 2880, 665	C–H bending vibration
1421, 1322	OH, CH vibration in the ring
2877,1421, 1322, 1249	CH_2 in pyranose ring
1422	Vibration of C-OH group
1724, 1580, 1395	C=O, Stretching vibration C=O
1646, 1642	C=O in amide I group
1653, 1657, 1650	Amide I, Stretching vibration of amide I
1381	CH_3 in amide group
1096, 1030, 1249, 1075,1033	C–O group in amide group, C-O vibration stretching
1580, 1562, 1552	Amide II,Amide II band due to N–H bending (Amide II)
1320	Amide III
1320, 1590	Amino characteristic peaks
1593	NH_2 bending vibration in amino group
1417	Coupling C-N axial stretching
1152, 1153	–C–O–C– bridge
1153-897	Polysaccharide, C-O and C-O-C
1085	C-O-C bond
1065, 1150, 1024	C-O-C symmetric, C-O-C asymmetric vibration
1380	Stretching vibration of methyl group
893, 1153	Saccharide structure

* (de Britto & Campana-Filho 2007; Zawadzki & Kaczmarek 2010; Bui et al. 2011; Caridade et al. 2013; Yao et al. 2014; Maji et al. 2016)

A broad band (Figure 4.6) corresponding to water is visible in the ~3000 – 3500cm^{-1} range. With glass introduction, the water band shift to higher wavenumber and three distinct peak appears in the broad band. The triple peak with bands from 3175 cm^{-1} to ~3420cm^{-1} refers to high water content in silica glass (Efimov & Pogareva 2006). When glass content increases, the triple peaks increase in intensities (Davis & Tomozawa 1995).

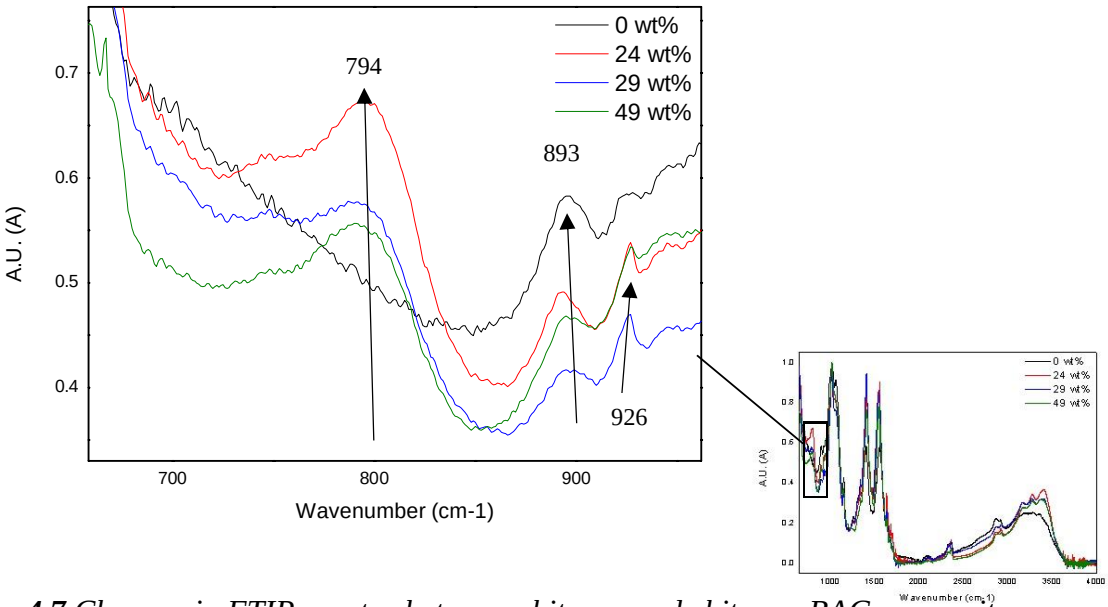

Figure 4.7 *Changes in FTIR spectra between chitosan and chitosan-BAG composite*

Figure 4.7 shows changes of the FTIR spectra of chitosan and chitosan-glass composites. With introducing bioactive glasses in the composite a new peak appears at ~ 793- 800 cm^{-1}. The peak correspond to the presence of BAG, specifically to Si-O-Si bond (Cerruti et al. 2005b; Caridade et al. 2013). This is due to symmetric stretching of Si-O-Si bridging oxygen (ElBadry et al. 2000). The peak corresponding to saccharide structure bond has higher intensity at 893 cm^{-1} in chitosan, and decrease in the presence of glass (Wanjun et al. 2005). The peak at 926 cm^{-1} is sharper in the BAG containing samples. This is related to the presence of both P-O and Si-O vibration (Cerruti et al. 2005b). All the bands show that addition of bioactive glass changes the chitosan conformation.

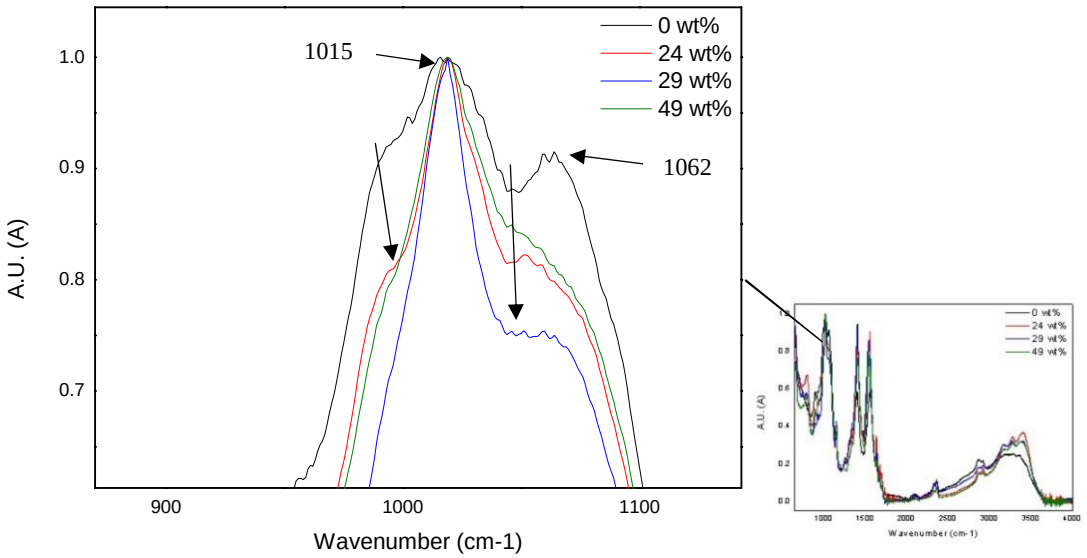

Figure 4.8 *Changes in FTIR spectra between chitosan and chitosan-BAG composite*

Changes in the highest peak of the spectra is shown as a zoomed graph in Figure 4.8. The peak with highest intensity, centered at 1015 cm^{-1} is attributed to C–O and C–O–C vibrations (Zawadzki & Kaczmarek 2010). This band arises from the chitosan and stays at the same intensity when introduced to glass. With addition of the bioactive glass, the shoulders of the band decreases due to the interaction between glass and chitosan. A shoulder at ~1062 cm^{-1}, which disappears in presence of glass, corresponds to C – O – C vibrations (Silva et al 2012). Chitosan FTIR spectra exhibit shoulders around the main peak, and with addition of the glass these shoulders decrease in intensity. Addition of the BAG causes change in the chitosan conformation.

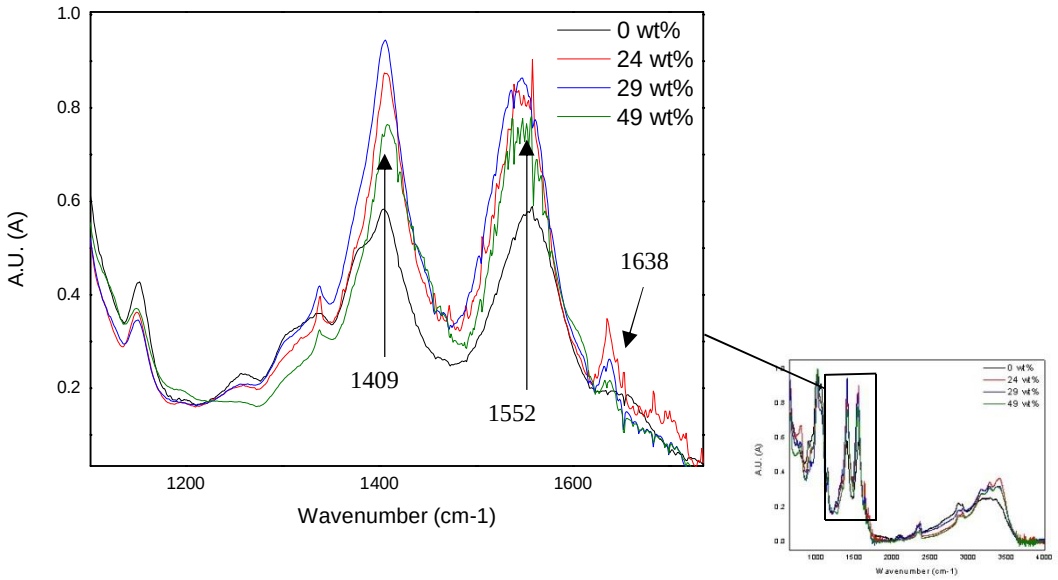

Figure 4.9 *Changes in double peak bands between chitosan and chitosan-BAG composite*

Figure 4.9 shows changes in the double bands of the spectra. The double peak at ~1404 – 1409 cm^{-1} is attributed to the presence of carbonate (CO_3^{2-}) as well as C-O bond, and the band peaking at 1552 cm^{-1} corresponds to amide II band due to N–H bending respectively (Bui et al. 2011; Yao et al. 2014; Zawadzki & Kaczmarek 2010). As glass is introduced to the chitosan, interaction between amide group and glass takes place (Bui et al. 2011). Both of these peaks increase in the presence of glass. The signal of composites 24wt-% and 49wt-% is noisy at the second peak, but a clear difference between samples can be seen. The higher the glass percentage in the composite sample the higher the intensity of the peaks. However, chitosan-BAG 49wt-% is lower in intensity. A small peak at ~1638 cm^{-1} that sharpens in composite samples, corresponds to carbonate, and it is absent in pure chitosan. This is a result of interconnection between chitosan and bioactive glass (Maji et al. 2016). This peak has very low intensity in the highest BAG glass containing scaffolds. this can be attributed to agglomeration of glass particles and reduction in the chitosan – BAG interactions.

4.3 *In-vitro* dissolution

Changes in the sample properties after *in vitro* dissolution test were thereafter also monitored, and the results are also presented in the following sections. Figure 4.10 present photographs of some samples after immersion in TRIS. At all time-points, at least one or two of the samples presented bubble formation as a result of sample swelling. Bubble sizes in the sample differed from a few millimetres to few centimetres. As a consequence, samples became deformed, even after drying. This is probably due to the penetration of water through the pores of the scaffolds during immersion and to the high swelling characteristic of chitosan.

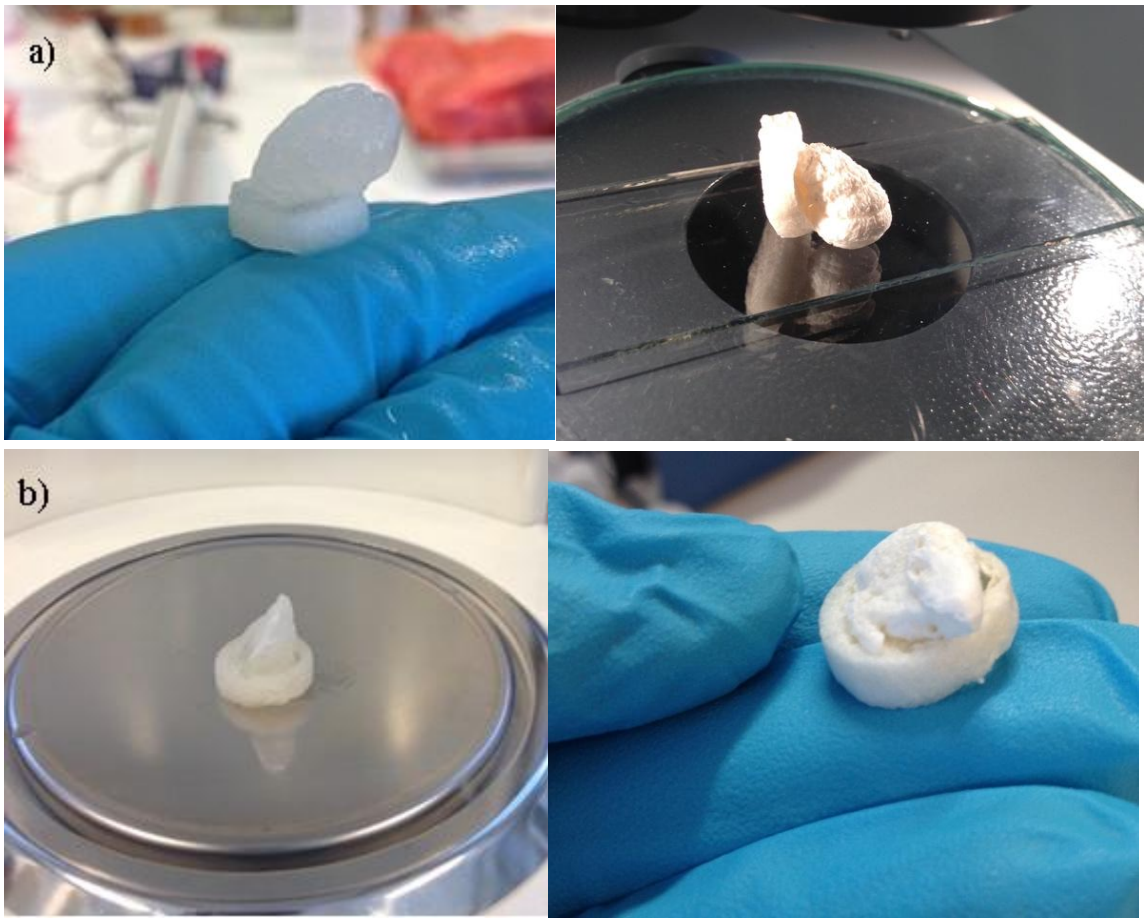

Figure 4.10 *Photograph of composites samples after immersion in TRIS. A) 24wt-% sample after 24h immersion and dried. b) 29wt-% sample after 72h after immersion and dried.*

4.3.1 pH measurement

pH measurement after *in vitro* dissolution is an indicator of material degradation during immersion test (Cerruti et al. 2005a). pH was measured at 37°C. The average of the three parallel samples is shown in Figure 4.11 for the full immersion time along with the standard deviation. Figure 4.12 shows the pH change over the first two weeks.

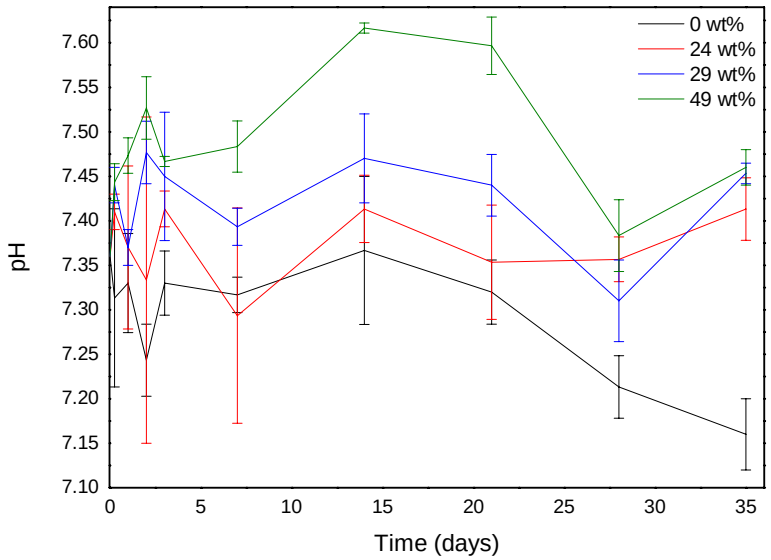

Figure 4.11 *pH of the TRIS solution as a function of immersion time (0-35 days)*

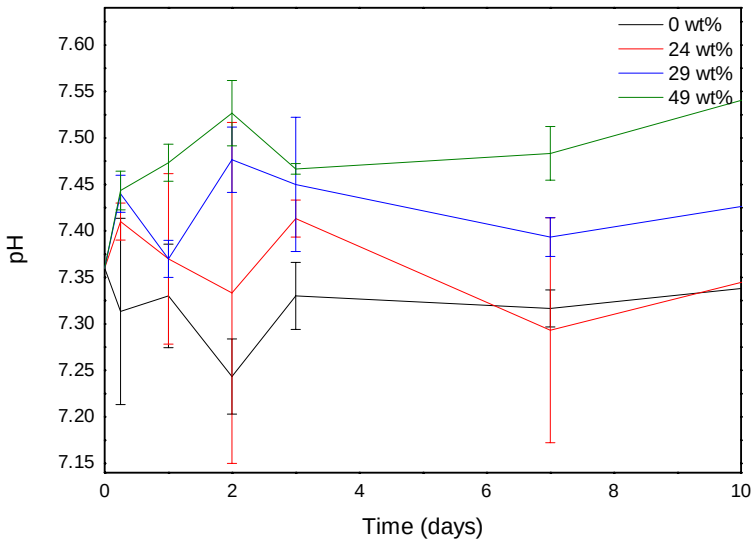

Figure 4.12 *pH of the TRIS solution as a function of immersion time (0-10 days)*

First and foremost, one should note that the accuracy of the measurement is higher than those typically reported for massive samples. This is partly due to the variance from samples to samples, where the porosity of samples cannot be fully controlled. The chitosan control showed limited decrease in pH over the first two weeks of immersion after which the pH started to drop. Within the first two weeks of immersion a slight increase in pH can be seen for the composite materials. The pH is higher with increasing the bioactive glass content. This was expected and indicates that the glass degrades *in vitro*. Na^+/H^+ ion exchange causes pH rise in the experiment, as first step of glass degradation. (Cerruti et al. 2005a; Boccaccini

et al. 2010). Indeed, it has been previously reported that pH rises immediately after scaffold with BAG is immersed in the solution (Cerruti et al. 2005a). However, for longer immersion time the pH decreases. This can be attributed to the degradation of chitosan within the media as well as a decrease in the dissolution of the bioactive glass. The graph shows that the higher the glass content the higher the pH up to 20 days indicating proper glass dissolution within the immersion solution.

4.3.2 Mass loss and water absorption

The average water absorption as a function of immersion time is reported in Figure 4.13. As can be seen from Figure 4.10 most samples presented a bubble at the centre of the scaffold. This was attributed to the water penetration within the scaffolds.

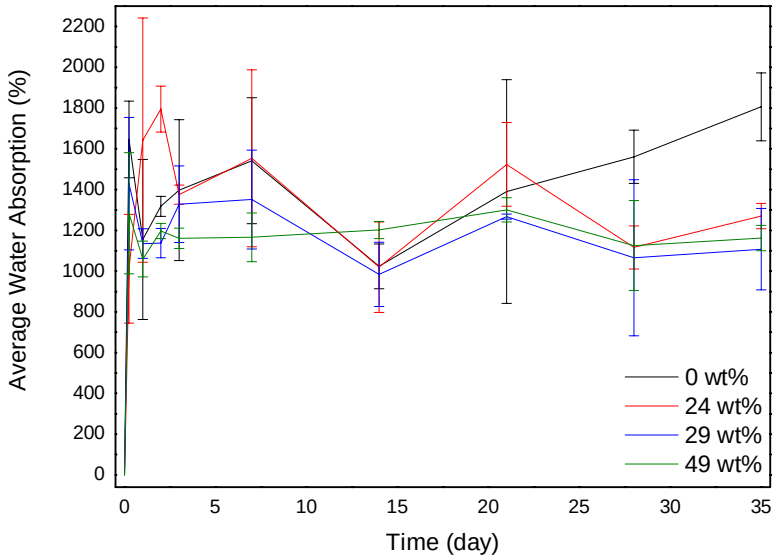

Figure 4.13 *Average water absorption (%) of the scaffolds during 35 days dissolution test in TRIS*

All samples exhibit large water absorption of 1200 to 1600% soon after being immersed in TRIS buffer solution. Similar behaviour was reported in previous study (Ruiz-Caro & Veiga-Ochoa 2009). Collagen/chitosan porous scaffolds showed improved biostability, when examined for skin tissue engineering. However, in that particular study the increase in water absorption occurs over brief time (30 min) and then the water absorption decreases. In our case the samples maintain the liquid within its structure for as long as the immersion was tested. Chitosan has high ability to absorb water, and this has been reported in the literature (Ren et al. 2005b; Soumen 2012). This can be explained by the fact that chitosan is hydrophilic and diffusion of water is faster than degradation. Material matrices first swell and then degrade (Ren et al. 2005b).Within the accuracy of the measurement no differences in water absorption could be detected with respect to the glass content. Only at the longest immersion time the pure chitosan samples seem to have higher water retention than the

composites. During this study only a few samples showed signs of degradation by visual observation, for instance in the centre of the discs. Figure ***4.14*** shows mass loss of the samples during 35 days *in vitro* immersion test in TRIS buffer solution.

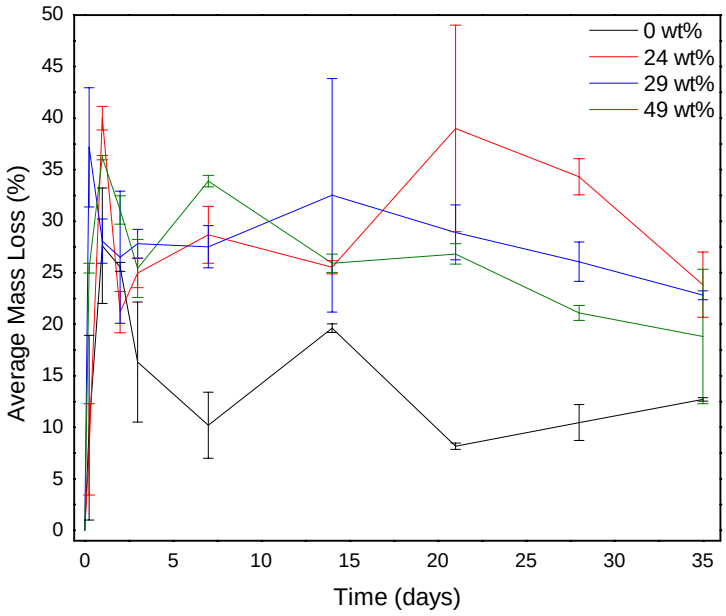

Figure 4.14 *Average mass loss of the scaffolds as a function of immersion time in TRIS*

From Figure 4.14 it can be observed that a steep mass loss occurred within the first two weeks of immersion, after which the mass loss decreased. While it is unlikely, in this study, this could mean that after the substantial mass loss of the chitosan control, a reactive layer formed at the surface of the material leading to a mass gain for longer immersion time (when compared to the 48h time point). This is not expected from pure chitosan but could very well happen for the composite material. Indeed, the dissolution of bioactive glasses may lead to the precipitation of a reactive layer. The increase in mass loss followed by a decrease in the mass loss should be investigated further. However, one can note that at the longest immersion time, the chitosan control has lost about 15% of its original weight, which is in agreement with study done by Thein-Han & Misra (Thein-Han & Misra 2008). Furthermore, all glass containing scaffolds seem to exhibit similar weight loss within the accuracy of the measurement. The weight loss is found to be higher than the one for chitosan control. This could be attributed to the heavy dissolution of the glass particles.

4.3.3 Calcium release

One very important indicating parameter for bioactivity of the bioactive glass is measuring calcium release of samples after being immersed in physiological medium (Caridade et al. 2013). In this study, samples were immersed in TRIS buffer solution, meaning there were no substances in the immersed solution to promote calcium release or formation. However,

working with bioactive glass allows to expect that there should be calcium formation/release over *in vitro* immersion period. Figure 4.15 present the calcium concentration in the immersion liquid as a function of immersion time.

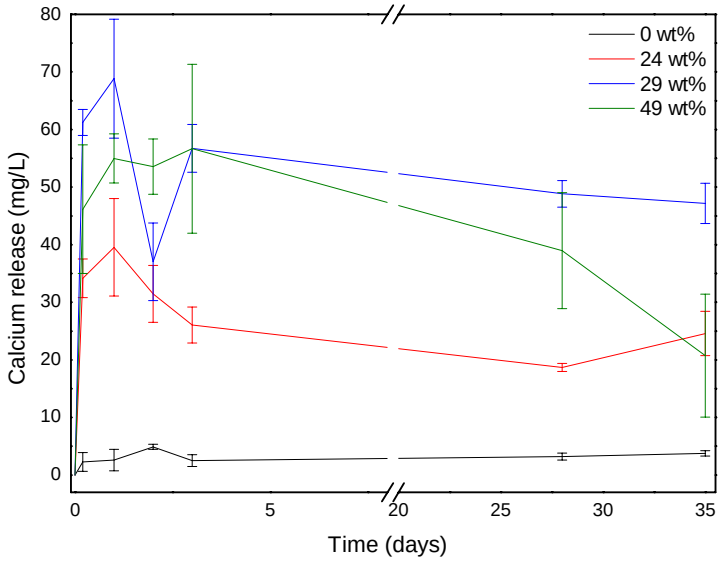

Figure 4.15 *Calcium release of the scaffolds after immersion in TRIS*

Calcium release of the chitosan control is almost constant as a function of immersion time. This confirms that no calcium was present neither in the TRIS buffer solution nor in the raw materials used to produce the chitosan scaffolds. Calcium release was high at the beginning of the *in vitro* dissolution test for all composite types, suggesting that there is a rapid calcium release at the beginning of the test. After 6 hours of immersion, calcium concentration goes to 34mg/L for 24wt%, 61mg/L for 29wt-% and 46mg/L for 49wt-%. Calcium release continues to increase after 24hours to 39mg/L, 68mg/L and 54mg/L for 24wt-%, 29wt-% and 49wt-% chitosan-BAG composites, respectively. Chitosan-BAG 49wt-% has lower calcium release results compared to the composite containing 29wt-%. Lower calcium release content of chitosan-BAG 49wt-% can be explained by smaller pore size in the sample. Indeed, as shown in the optical microscope image Figure 4.4, this sample has smaller pore size compared to other samples. Smaller pore size cannot facilitate Ca^{2+} ion transportation as well as for samples having bigger pore size. Calcium release of the chitosan-BAG composite 49wt-% continues to rise by three days after immersion test, and until two days for chitosan-BAG 24wt-%, but decreases towards the end of the *in vitro* dissolution test. Same behaviour has been reported in the literature. Increase is related to the release of available calcium content from bioactive glass in the dealkalization process. For longer immersion time Ca^{2+} release decreases for all composites. This indicates that calcium is being consumed, most probably during precipitation of a calcium phosphate layer. (Bui et al. 2011; Caridade et al. 2013)

4.3.4 Structural properties

To analyse changes in the scaffolds' structure after *in vitro* dissolution test, samples were studied using FTIR. Each sample is presented in a separate figure to detect structural changes during immersion test period of that particular sample. Results at 0 hour, 24 hours, 72 hours and 3 weeks after immersion are shown in this section. Figure 4.16 shows the FTIR spectra recorded for the pure chitosan scaffold when immersed in TRIS buffer solution.

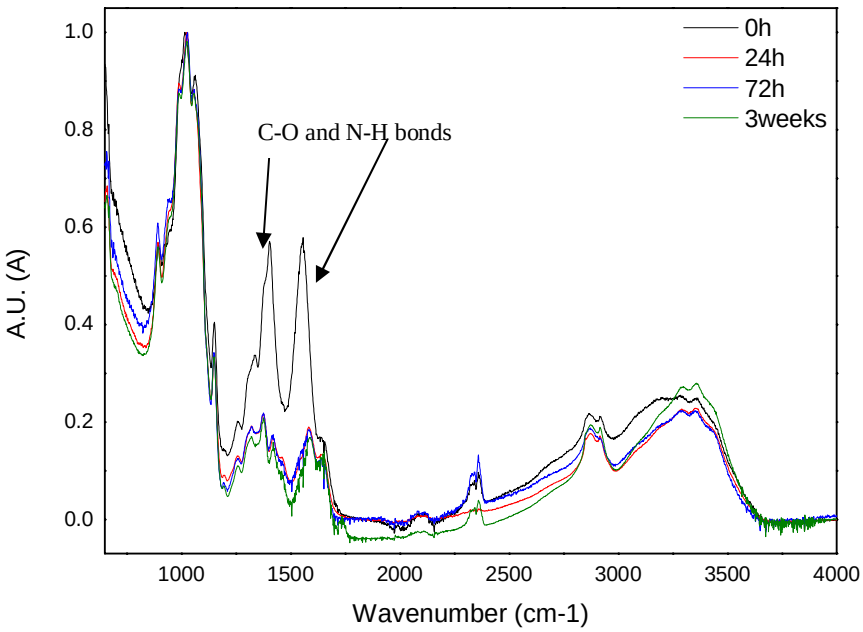

Figure 4.16 *FTIR spectra of the pure chitosan scaffolds immersed for up to 3 weeks*

There is a decrease in intensity of the double peak at 1400 – 1552 cm^{-1}, when chitosan is immersed in the TRIS solution. After 24 hours of immersion, C–O bond and N–H bond of amide II decreased in intensity, suggesting that they have degraded during the immersion test (Bui et al. 2011; Yao et al. 2014; Zawadzki & Kaczmarek 2010). Structural changes between 24 hours and 72 hours are not noticeably different. However, after 3 weeks in TRIS other bands discussed in section 4.2.4 decrease in intensity. The peak in the 3496– 3440 range attributed to O–H vibration increases in intensity (Efimov & Pogareva 2006). Degradation of the chitosan structure starts already before 24 hours of immersion in the TRIS. Obtained spectra suggests, that first C–O bonds of the polymer chain and N–H bonds are broken due to degradation of chitosan.

Figure 4.17 presents the FTIR spectra of the chitosan-BAG 24wt-% at various immersion times.

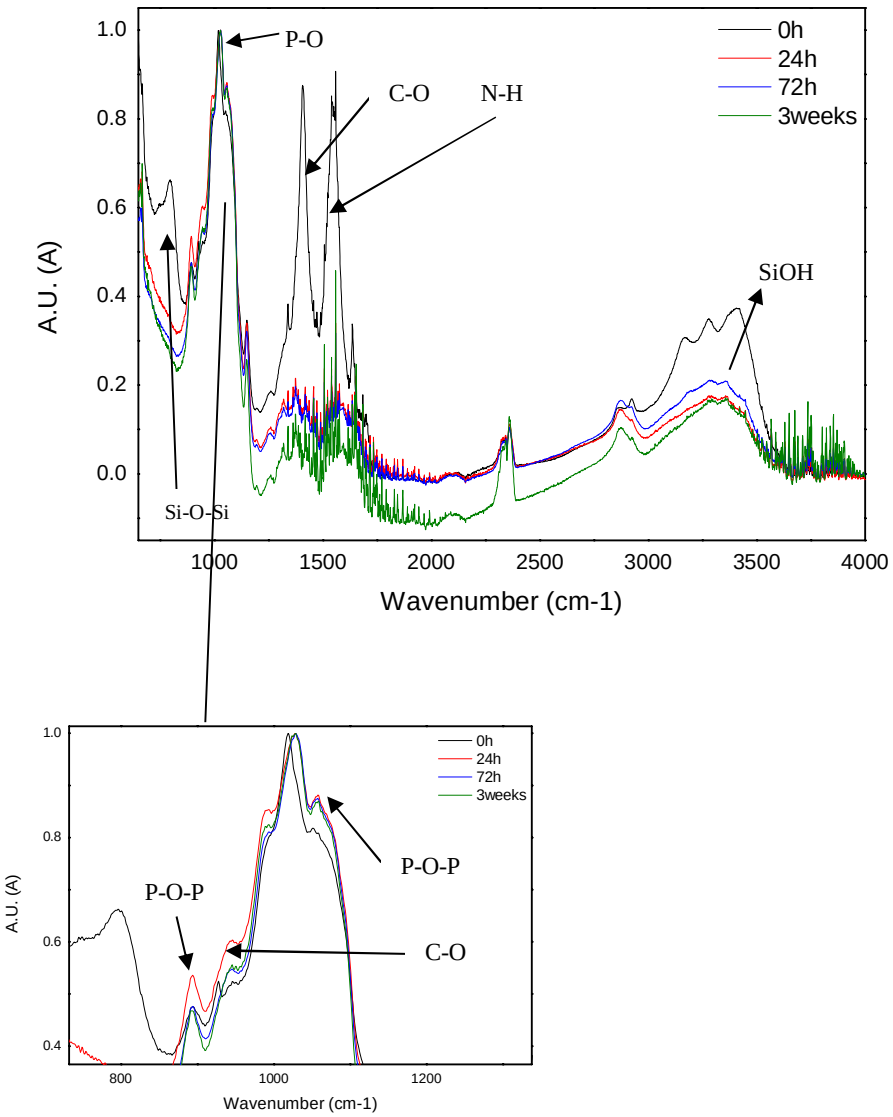

Figure 4.17 *FTIR spectra of the 24wt% composites scaffolds as a function immersion time.*

In the case of chitosan-BAG 24wt-%, the change compared to 0 day is clearly visible, as shown in Figure 4.17. The band corresponding to Si–O–Si and presence of silica disappears 24 hours after immersion (Caridade et al. 2013; Cerruti et al. 2005b). This confirms the breaking of Si–O–Si bridging that links to formation of silica-rich layer on the surface of the scaffold (Bui et al. 2011). The highest band at 1028 cm^{-1} arising from PO_4 referring to presence of PO_2 group symmetrical stretching (ElBatal et al. 2003; Maji et al. 2016). The peak becomes double shouldered referring to P–O–P asymmetric vibration at intensity of 893cm^{-1} and 1056 cm^{-1} (ElBadry et al. 2000). C–O and at intensity of 944 cm^{-1} arises from the carbonate formation, indicating formation of the carbonated hydroxycarbonate layer

(ElBatal et al. 2003; Bui et al. 2011). The double band corresponding to chitosan structure (C–O and N–H bonds at 1400 – 1552 cm^{-1}) decreases in intensity, referring to the chitosan compounds degradation. The longer the test period, the lower is the intensity of that band. It is noticeable that at the 3 week-time point has IR bands with lower intensity compared to other time points. Lower intensity of the peaks as a function of immersion time is a result of degradation of material. Triple bond formed by Si and water has disappeared and drops in intensity, because Si bonds are broken down to form silanol (SiOH) on the surface of the scaffold (Bui et al. 2011).

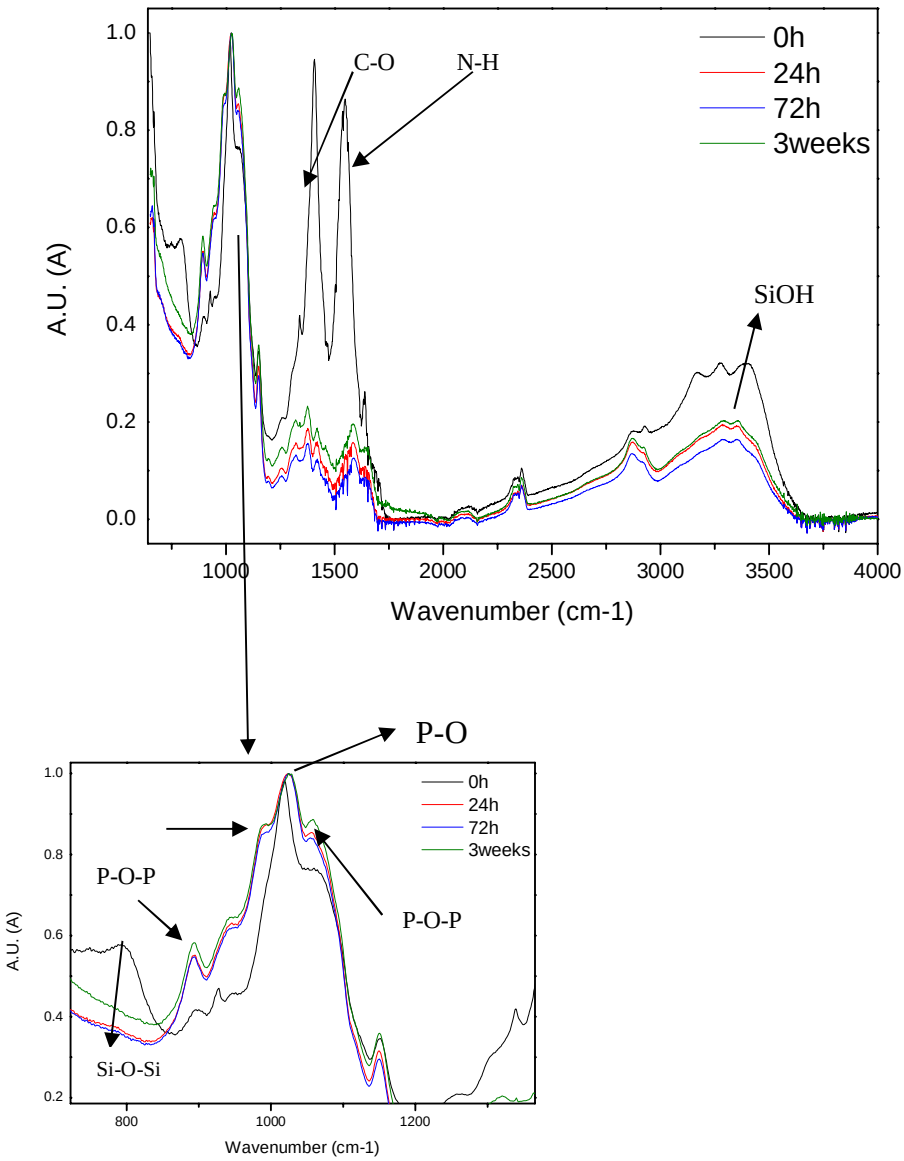

Figure 4.18 *FTIR spectra of the 29wt% composite as a function of time*

As for every other sample type, also double peak of the chitosan-BAG 29wt% has decreased in intensity remarkably, as shown in Figure 4.18. The low wavenumber range of the spectra has been zoomed, and it shows that smaller peak corresponding to Si–O–Si has disappeared with increasing immersion time. Phosphate band at 1022 cm^{-1} has become sharper and increased in intensity forming shoulders after being immersed in TRIS (Maji et al. 2016). The longer the immersion time the higher the intensity, suggesting that there is some phosphate layer formation in the scaffold. The shoulder at 890 cm^{-1} that corresponds to stretching vibration C–O–C group of chitosan rising intensity. The second shoulder at ~930 cm^{-1} corresponds to the Si–O bond (Bui et al. 2011). For this composite, FTIR spectra of the 3 week is higher in intensity compared to the spectra at 24 hours and 72 hours, which is opposite behaviour to chitosan-BAG 24wt-%. this can be related to the technique used. Indeed, FTIR when used in ATR mode, lies in the amount of structural units in contact with the diamond crystal. As it is expected that the Ca-P layer formation is not homogeneous across the samples, variation in the intensity of the peaks are to be expected.

Nevertheless, the disappearance of the bands relates to the silica structure as well as the decrease in intensity of the C–O and N–H bonds clearly indicate that both glass and natural polymers degrade over time. The appearance of vibrations attributed to phosphate and carbonate vibration tend to support the hypothesis that upon glass degradation, a calcium phosphate layer, close to a hydroxyapatite structure, precipitate at the surface of the composite.

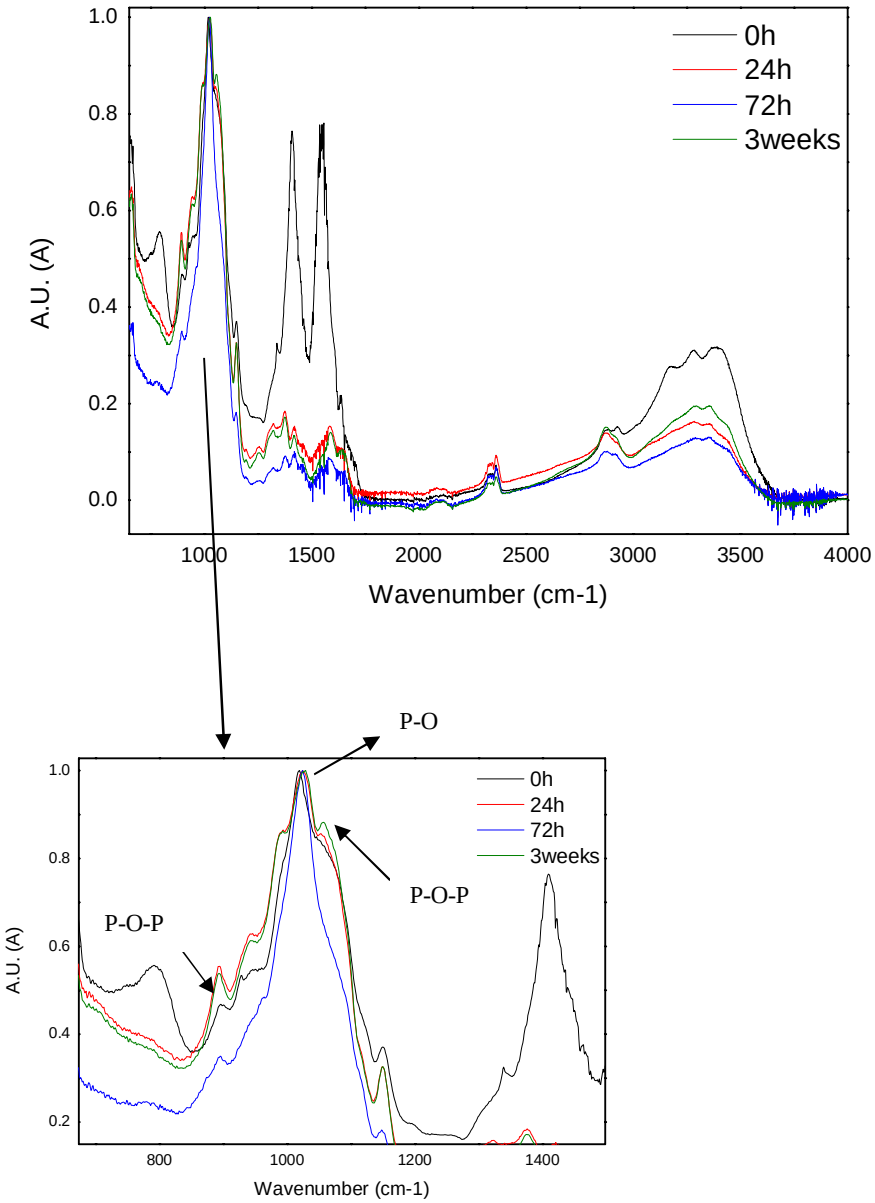

Figure 4.19 *FTIR spectra of the 49wt% composite as a function of immersion time*

Figure 4.19 introduces the change in the chitosan-BAG c 49wt% composite' structure during *in vitro* dissolution test. As for other composite types, the P-O band presents two shoulders after immersion in TRIS. The FTIR spectra of samples immersed for 72 hours has sharpest phosphate peak at 1022–1028cm^{-1} (ElBadry et al. 2000; Maji et al. 2016). Surprisingly, 72hours has spectra lower in intensity compared to 24hours and 3weeks, which might be due to uneven Ca-P precipitation and/or Ca-P dissolution due to the decrease in local pH upon chitosan degradation. Both hypothesis require more investigation to be confirmed.

In vitro dissolution test was done for 1-5 weeks, and there was no significant difference in the structure of the scaffolds. FTIR analysis shows that most of the change in the material

happens already before 24 hours, suggesting that scaffold dissolution should be studied using shorter time intervals. In the TRIS solution there was no calcium nor phosphate to promote hydroxyapatite layer formation, and all the apatite formation is coming from the bioactivity of the glass. Bands arising from phosphate and carbonate groups allows to predict that formation of hydroxyapatite or apatite layer during this study was detected by FTIR analysis.

4.3.5 Mechanical properties

After *in vitro* dissolution testing, wet and dry mechanical testing was performed by compressing the samples to 50% of their height. Scaffolds were shown to recover to their original shape, during testing of wet samples, in a few minutes, which is suggestive of their elastic properties. Figure 4.20 shows the compressive strength as a function of immersion time.

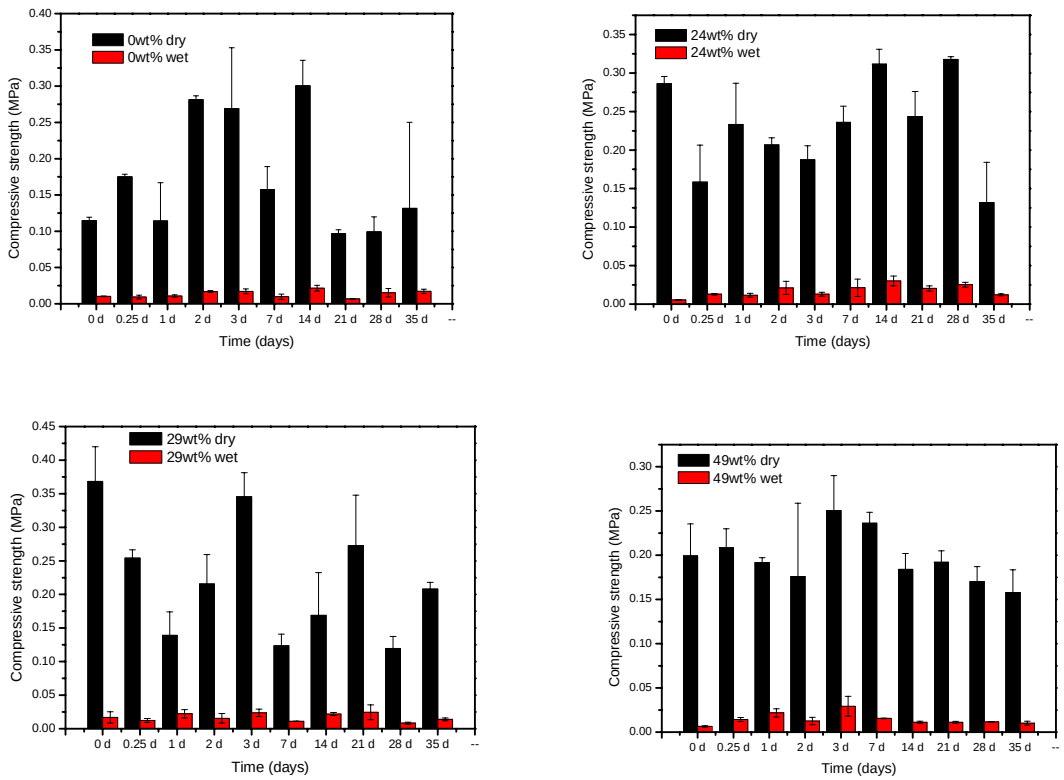

Figure 4.20 *Compressive strength of wet and dry samples during in vitro dissolution test*

From the figures one important observation is that wet samples shows low compression strength compared to the dry ones. Wet compression mimics more closely the environment the device is intended to be used in. The wet compressive strength is found to remain constant as a function of immersion time and within the accuracy of the measurement. The composite samples, however, tend to show a maximum at 14 days, 21 days and 3 days of immersion for samples containing 24, 29 and 49 wt-% of bioactive glass, respectively. This could correlate with the precipitation of the calcium phosphate reactive layer which will, most likely form

within the pores and increase the compressive strength at 50% deformation. As seen in the FTIR it is possible that the lower pH, at longer immersion time, or the chitosan degradation wash away the reactive layer, leading to a successive decrease in the compressive strength.

When the samples were dried, the change in the compressive strength was not monotonic. Nevertheless, a maximum in compressive strength at 3 or 14 days depending on the glass content could be extrapolated from Figure 4.20. This can also be due to the calcium phosphate precipitation and further chitosan degradation.

The large errors of measurement are attributed to the uneven surface post-immersion. Indeed, as shown in Figure 4.10, bubbles tend to form at the centre of the specimen making the measurement more unreliable.

Figure 4.21 shows the Young's modulus of samples tested in dry and wet conditions, as a function of immersion time.

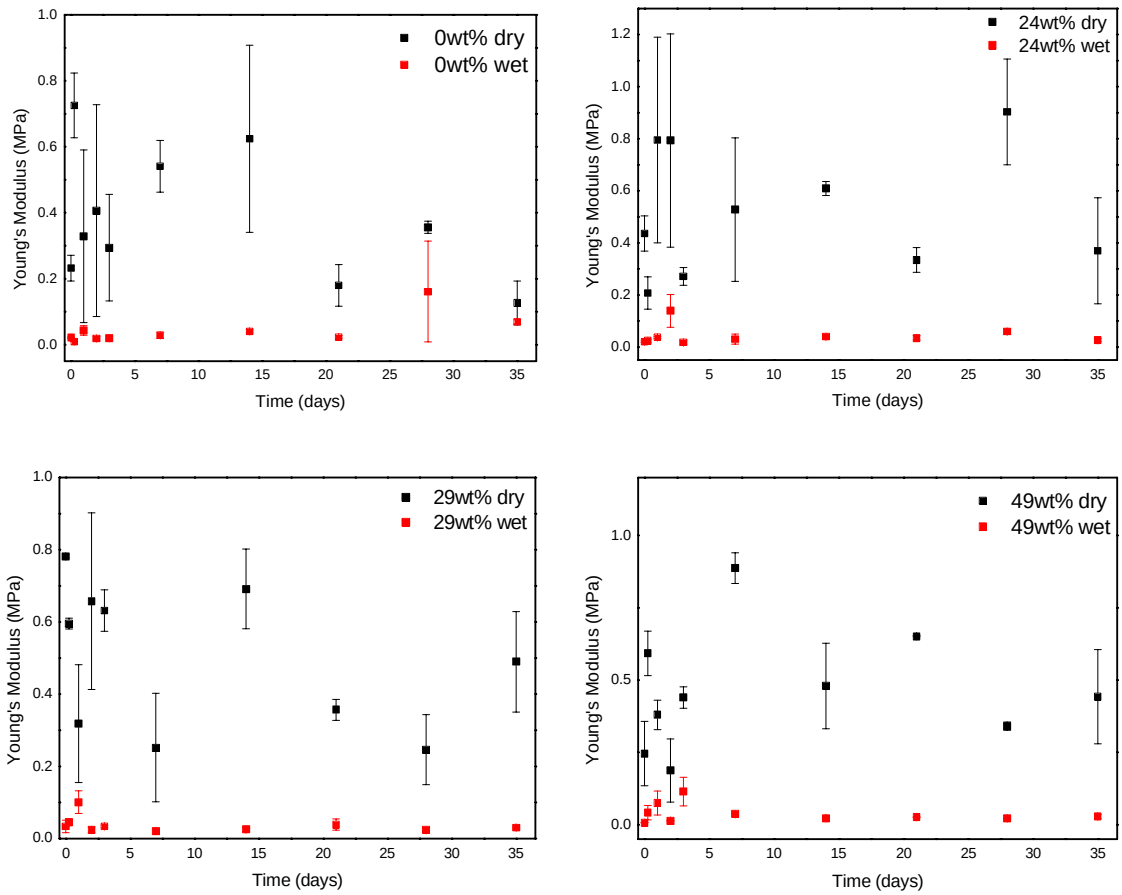

Figure 4.21 *Young's Modulus of wet and dry samples during in vitro dissolution test*

The Young's modulus was calculated from the same curves obtained for the tensile strength measurement. Not all the samples had plastic deformation during compression test. As shown in the Figure 3.3, location of the elastic curve differs, consequently the Young's modulus differs even between the duplicates causing large variation between them. Higher modulus

i.e. more strength is necessary to compress dry samples compared to wet ones. Chitosan control has the highest Young's modulus at 0.73 MPa, where composites have highest modulus between 0.72-0.91MPa. Increase in modulus with adding glass is expected, as the Young's modulus of the glass is higher than the polymer, therefore the Young's modulus should increase. However, there is a small increase in modulus of composites compared to chitosan control, which is opposite to expectation. No literature was found to report similar mechanical behaviour found in this study. In order to obtain reliable results for mechanical properties, a higher number of replicates should have been used. Most importantly, suitable fabrication of the chitosan- glass samples would lead to overall more reliable and comparable results.

5. CONCLUSIONS

The aim of this work was to fabricate a composite scaffold from a natural polymer i.e. chitosan, and bioactive glass S53P4 and to study the effect of the bioactive glass on the mechanical properties of chitosan scaffolds, as well as formation of apatite layer after *in vitro* dissolution test.

While the addition of bioactive glass did not lead to significant change in the swelling behaviour of the material the following was observed:

1. The pH was found to increase upon glass dissolution and remain within physiological condition during dissolution, even once the chitosan start degrading.
2. The average mass loss increases when glass particles are introduced within the chitosan due to glass degradation
3. Calcium is being released within the solution due to glass dissolution.
4. The Ca^{2+} concentration decreases at long immersion time probably due to hydroxyapatite precipitation
5. Hydroxyapatite precipitation was confirmed by FTIR analysis
6. The compression strength was found to increase with adding glass particles

However, few observations should be taken into consideration. The large size of the glass particles led to sinking of the particles and therefore inhomogeneous composite structure. The heavy swelling of chitosan inhibits accurate investigation of mechanical properties.

The high porosity of the samples and its assumed bioactivity are promising in bone application. Furthermore, the use of chitosan and S53P4 bioactive glass composites may allow their use in drug delivery and as bioactive materials in soft or hard tissue engineering.

REFERENCES

Boccaccini, A.R., Erol, M., Stark, W.J., Mohn, D., Hong, Z. & Mano, J.F. (2010). Polymer/bioactive glass nanocomposites for biomedical applications: A review, Composites Science and Technology, Vol. 70(13), pp. 1764-1776.

Bui, X., Oudadesse, H., Le Gal, Y., Mostafa, A. & Cathelineau, G. (2011). Microspheres of Chitosan-Bioactive Glass for Application in Orthopedic Surgery. In vitro experiment, Recent Researches in Modern Medicine, pp. 359-3667.

Caridade, S.G., Merino, E.G., Alves, N.M., Bermudez, V.D.Z., Boccaccini, A.R. & Mano, J.F. (2013). Chitosan membranes containing micro or nano-size bioactive glass particles: Evolution of biomineralization followed by in situ dynamic mechanical analysis, Journal of the Mechanical Behavior of Biomedical Materials, Vol. 20pp. 173-183.

Cerruti, M.G., Greenspan, D. & Powers, K. (2005a). An analytical model for the dissolution of different particle size samples of Bioglass® in TRIS-buffered solution, Biomaterials, Vol. 26(24), pp. 4903-4911.

Cerruti, M., Greenspan, D. & Powers, K. (2005b). Effect of pH and ionic strength on the reactivity of Bioglass® 45S5, Biomaterials, Vol. 26(14), pp. 1665-1674.

Davis, K.M. & Tomozawa, M. (1995). Water diffusion into silica glass: Structural changes in silica glass and their effect on water solubility and diffusivity, Journal of Non-Crystalline Solids, Vol. 185(3), pp. 203-220.

de Britto, D. & Campana-Filho, S.P. (2007). Kinetics of the thermal degradation of chitosan, Thermochimica Acta, Vol. 465(1-2), pp. 73-82.

Efimov, A.M. & Pogareva, V.G. (2006). IR absorption spectra of vitreous silica and silicate glasses: The nature of bands in the 1300 to 5000 cm− 1 region, Chemical Geology, Vol. 229(1–3), pp. 198-217.

ElBadry, K.M., Moustaffa, F.A., Azooz, M.A. & ElBatal, H.F. (2000). Indian Journal of Pure & Applied Physics, Vol. 38pp. 741-761.

ElBatal, H.A., Azooz, M.A., Khalil, E.M.A., Soltan Monem, A. & Hamdy, Y.M. (2003). Characterization of some bioglass–ceramics, Materials Chemistry and Physics, Vol. 80(3), pp. 599-609.

Escobar-Sierra, D.M., Martins, J. & Ossa-Orozco, C.P. (2015). Chitosan/hydroxyapatite scaffolds for tissue engineering manufacturing method effect comparison, Revista Facultad de Ingenieria, Vol. 1(75), pp. 24-35.

Hench, L.L. (1991). Bioceramics: From Concept to Clinic. Journal of the American Ceramic Society, Vol. 74(7), pp. 1487-1510.

Georgieva, V., Zvezdova, D. & Vlaev, L. (2012). Non-isothermal kinetics of thermal degradation of chitosan, Chemistry Central Journal, Vol. 6(1), .

Jayakumar, R., Menon, D., Manzoor, K., Nair, S.V. & Tamura, H. (2010). Biomedical applications of chitin and chitosan based nanomaterials—A short review, Carbohydrate Polymers, Vol. 82(2), pp. 227-232.

Jin, H.-., Lee, C.-., Lee, W.-., Lee, J.-., Park, H.-. & Yoon, S.-. (2008). In-situ formation of the hydroxyapatite/chitosan-alginate composite scaffolds, Materials Letters, Vol. 62(10-11), pp. 1630-1633.

Langer, R. & Vacanti, J.P. (1993). TISSUE ENGINEERING, Science, Vol. 260pp. 920-926.

Madihally, S.V. & Matthew, H.W.T. (1999). Porous chitosan scaffolds for tissue engineering, Biomaterials, Vol. 20(12), pp. 1133-1142.

Maji, K., Dasgupta, S., Pramanik, K. & Bissoyi, A. (2016). Preparation and Evaluation of Gelatin-Chitosan-Nanobioglass 3D Porous Scaffold for Bone Tissue Engineering, International Journal of Biomaterials, Vol. 2016.

Massera, J. (2015). Bioactive glasses: Silicate and phosphate-based glasses, ELT-73106-01 Bioceramics and their clinical applications.

Massera, J., Fagerlund, S., Hupa, L. & Hupa, M. (2012). Crystallization mechanism of the bioactive glasses, 45S5 and S53P4, Journal of the American Ceramic Society, Vol. 95(2), pp. 607-613.

Orava, E., Korventausta, J., Rosenberg, M., Jokinen, M. & Rosling, A. (2007). In vitro degradation of porous poly(dl-lactide-co-glycolide) (PLGA)/bioactive glass composite foams with a polar structure, Polymer Degradation and Stability, Vol. 92(1), pp. 14-23.

Peter, M., Binulal, N.S., Soumya, S., Nair, S.V., Furuike, T., Tamura, H. & Jayakumar, R. (2010). Nanocomposite scaffolds of bioactive glass ceramic nanoparticles disseminated chitosan matrix for tissue engineering applications, Carbohydrate Polymers, Vol. 79(2), pp. 284-289.

Pishbin, F., Simchi, A., Ryan, M.P. & Boccaccini, A.R. (2011). Electrophoretic deposition of chitosan/45S5 Bioglass® composite coatings for orthopaedic applications, Surface and Coatings Technology, Vol. 205(23-24), pp. 5260-5268.

Rahaman, M.N., Day, D.E., Sonny Bal, B., Fu, Q., Jung, S.B., Bonewald, L.F. & Tomsia, A.P. (2011). Bioactive glass in tissue engineering, Acta Biomaterialia, Vol. 7(6), pp. 2355-2373.

Ravi Kumar, M.N.V. (2000). A review of chitin and chitosan applications, Reactive and Functional Polymers, Vol. 46(1), pp. 1-27.

Ren, D., Yi, H., Wang, W. & Ma, X. (2005a). The enzymatic degradation and swelling properties of chitosan matrices with different degrees of N-acetylation, Carbohydrate research, Vol. 340(15), pp. 2403-2410.

Ren, D., Yi, H., Wang, W. & Ma, X. (2005b). The enzymatic degradation and swelling properties of chitosan matrices with different degrees of N-acetylation, Carbohydrate research, Vol. 340(15), pp. 2403-2410.

Ruiz-Caro,R., Veiga-Ochoa, M.D. (2009).Characterization and dissolution study of chitosan freeze-dried system for drug delivery controlled release. Molecules 2009, 14, 4370-4386, doi:10.3390/molecules14114370

Soumen, J. (2012). Designing of Chitosan-Based Scaffolds for Biomedical Applications, Doctor of Philosophy, 1-43 p.

van Gestel, N.A.P., Geurts, J., Hulsen, D.J.W., van Rietbergen, B., Hofmann, S. & Arts, J.J. (2015). Clinical applications of S53P4 bioactive glass in bone healing and osteomyelitic treatment: A literature review, BioMed Research International, Vol. 2015pp. 1-12.

Vroman, I. & Taghzert, L. (ed.). (2009). Biodegradable Polymers. 2nd ed. 307-344 p.

Thein-Han, W.W., Misra, R.D.K. (2008). Biomimetic chitosan–nanohydroxyapatite composite scaffolds for bone tissue engineering, Acta Biomaterialia. Vol. 5(4), pp.1182-1197.

Wanjun, T., Cunxin, W. & Donghua, C. (2005). Kinetic studies on the pyrolysis of chitin and chitosan, Polymer Degradation and Stability, Vol. 87(3), pp. 389-394.

Yao, Q., Nooeaid, P., Detsch, R., Roether, J., Dong, Y., Goudouri, O., Schubert, D. & Boccaccini, A. (2014). Bioglass/chitosan–polycaprolactone bilayered composite scaffolds intended for osteochondral tissue engineering, Journal of Biomedical Materials Research - Part A, Vol. 102(12), pp. 4510-4518.

Zawadzki, J. & Kaczmarek, H. (2010). Thermal treatment of chitosan in various conditions, Carbohydrate Polymers, Vol. 80(2), pp. 395-401.

Zhang, D., Leppäranta, O., Munukka, E., Ylänen, H., Viljanen, M.K., Eerola, E., Hupa, M. & Hupa, L. (2010). Antibacterial effects and dissolution behavior of six bioactive glasses, Journal of Biomedical Materials Research - Part A, Vol. 93(2), pp. 475-483.